Fermi National Accelerator Laboratory

FERMILAB-Pub-93/294-A
September 1993

Statistical Tests for the Gaussian Nature of Primordial Fluctuations Through CBR Experiments[1]

Xiaochun Luo

Departments of Physics and of Astronomy & Astrophysics
Enrico Fermi Institute, The University of Chicago, Chicago, IL 60637-1433
NASA/Fermilab Astrophysics Center, Fermi National Accelerator Laboratory, Batavia, IL 60510-0500

ABSTRACT

Information about the physical processes that generate the primordial fluctuations in the early universe can be gained by testing the Gaussian nature of the fluctuations through cosmic microwave background radiation (CBR) temperature anisotropy experiments. One of the crucial aspects of density perturbations that are produced by the standard inflation scenario is that they are Gaussian, whereas seeds produced by topological defects left over from an early cosmic phase transition tend to be non-Gaussian. To carry out this test, sophisticated statistical tools are required. In this paper, we will discuss several such statistical tools, including multivariant skewness and kurtosis, Euler-Poincare characteristics, the three point temperature correlation function, and the Hotelling's T^2 statistic defined through bispectral estimates of a one dimensional dataset. The effect of noise present in the current data is discussed in detail and the COBE 53 GHz dataset is analyzed. Our analysis shows that, on the large angular scale to which COBE is sensitive, the statistics are probably Gaussian. On the small angular scales, the importance of Hotelling's T^2 statistic is stressed, and the minimum sample size required to test Gaussianity is estimated. Although the current dataset

[1]Submitted to *Phys. Rev. D.*

Operated by Universities Research Association Inc. under contract with the United States Department of Energy

available from various experiments at half-degree scales is still too small, improvement of the dataset by roughly a factor of two will be enough to test the Gaussianity statistically. On the arcminute scales, we analyze the recent RING data through bispectral analysis, and the result indicates possible deviation from Gaussianity. Effects of point sources are also discussed. It is pointed out that the Gaussianity problem can be resolved in near future by ground-based or balloon-borne experiments.

1 Introduction

The cosmic structure formation problem is essentially an initial value problem: how did the universe generate the initial perturbations? In particular, one can divide the initial condition models into two clear classes: Gaussian or non-Gaussian? Cosmic inflation [1], on one hand, provides a natural way to generate Gaussian initial perturbations [2]; spontaneous symmetry breaking, on the other hand, will lead to the formation of topological defects [4] via Kibble mechanism [3], and the perturbations generated by topological defects can be characterized as non-Gaussian. Non-Gaussian perturbations also arise in various non-standard inflationary models [5]. Thus, a test of the Gaussian nature of the primordial perturbations will not only be helpful in discriminating different models for structure formation, but could also shed light on new physics that yield topological defects or special non-standard inflations in the early universe. Such a test is, therefore, very important and timely in today's cosmology.

There are two ways to carry out the test. One is from the statistics of the galaxy counts in a redshift survey [6]. However, since the density field we observe today has already gone through the "black-box" of non-linear gravitational evolution, one has to filter out this effect carefully to get a reliable estimate of primordial quantities [7]. In this paper, we will concentrate on the other approach, which is from the cosmic microwave background radiation (CBR) anisotropy experiments. The experiments measure the primeval density perturbations at redshift $z \sim 1000$. The density contrast is fairly small at this epoch. The Gaussian nature of the microwave background fluctuation directly reflects the nature of the primordial perturbations. This approach is promising, especially after COBE's detection [8] of the temperature anisotropies at large angular scales, and the continuing accumulation of data on smaller angular scales[9].

Prior to COBE's detection, studies on CBR were focused on determining the level of anisotropies. The Gaussianity test of the anisotropies was largely considered as a next-step problem and experimentally intractable. Few detailed studies [10] [11] on the statistics of the CBR anisotropies have been carried out except for the Gaussian case [12]. Now that the CBR anisotropies are detected [8][13], this next-step but important question should be brought into focus and we are optimistic that it can be resolved experimentally in near future. As we will show later, one doesn't need a full-sky coverage at

high angular-resolution to study the Gaussianity problem statistically.

There are several recent papers on statistical tests for Gaussianity [14][15][16]. To carry out the test through CBR experiments, two important feature have to be stressed. One is the instrumental noise which is present in all current experiments. One should have a clear understanding of the instruments and associated noise before attempting to decipher non-Gaussian signals from experiments. The other feature is the smoothing scale θ_s each experiment operates. Note that the angular size of the comoving horizon at decoupling epoch is $\theta_c \sim 2^\circ$ by assuming standard recombination [17]. Put this characteristic scale in mind, one can divide all CBR experiments into three categories: large scales ($\theta_s \gg \theta_c$), intermediate scales ($\theta_s \sim 1^\circ$) and small scales ($\theta_s \sim$ arcminutes). For large scale experiments [8][13], each measurement is a sum of anisotropies in several independent horizons, and one would expect the statistic to be close to a Gaussian simply by the virtue of central limit theorem [18][19]. For small scale experiments [20], we will show later that the data fails the Gaussian statistical tests. However, on arcminute scales, foreground source contaminations are important. The statistics of the data may not reflect the statistics of the CBR anisotropies at these scales. Intermediate scale experiments [21] are ideal for testing Gaussianity. Although the dataset available is still too small, as we will show in section 4, improvement of the dataset by roughly a factor of two will be able to test the Gaussinity of CBR statistically.

Several statistical tools are discussed in this paper. In section 2, we discuss the simplest tests of Gaussianity through the skewness and kurtosis of the one point distribution. Skewness and kurtosis are the normalized third and fourth moments of the distribution and they vanish for Gaussian distribution. Several physically motivated non-Gaussian probability distribution functions (PDFs) are considered, and effects of noise are discussed. To consider the possible correlation between the signal and noise, multi-variant skewness and kurtosis are introduced and their statistics are discussed. In section 3, one geometrical measure of the random field, the Euler-Poincare (EP) characteristic, is discussed and used to test Gaussianity. The statistics of the EP-characteristic and the effects of noise are discussed and we show that EP-characteristic is hardly a good discriminator between Gaussian and non-Gaussian fields when the noise is comparable to the signal. In section 4, we discuss using the three point correlation to test Gaussianity. Theoretical predictions in various models are discussed and we present

our analysis of COBE 53 Ghz data. The result is in good agreement with Gaussian assumption. In section 5, we discuss using Hotelling's T^2 statistic to test Gaussianity on intermediate angular scales ($\theta \sim 1°$). The minimum sample size to carry out the test is estimated and sampling technique are also discussed. Although the current dataset is still too small to carry out the Gaussianity test, improvement of the sample size by roughly a factor of two will be adequate. In section 6, we use the T^2 statistic to test RING dataset from OVRO [20] on small angular scales ($\sim$ arcminutes). It is found that the data is not consistent with Gaussian distribution. However, one cannot conclude that the CBR anisotropies are non-Gaussian on these scales because of the foreground source contaminations. In section 7, we discuss looking for a special non-Gaussian signal, the point-like CBR anisotropy, in small scale CBR experiments. The Gaussian nature of perturbations from inflation is shown in the appendix.

2 Skewness and Kurtosis of Noisy Data

The simplest tests of Gaussianity will be skewness μ_3 and kurtosis μ_4 [7] of the distribution of temperature anisotropies δ,

$$\mu_3 = m_3/\sigma^3, \quad \mu_4 = m_4/\sigma^4 - 3, \tag{1}$$

where m_3 and $\hat{m}_4$ are the third and fourth moments of the distribution, adn σ is the variance of δ. For Gaussian distribution, both μ_3 and μ_4 vanish. In this section, we discuss several physically motivated non-Gaussian distributions: exponential, log-normal and χ^2. As we expect, noise will blur the effects of non-Gaussian distribution. The skewness and kurtosis for these distributions are calculated both with and without noise. We also discuss the use of multivariant skewness and kurtosis in cases of noisy data and show how to estimate them from experimental data.

2.1 Skewness and Kurtosis of Non-Gaussian Signals

Coles and Barrow [10] have studied the statistics of a large class of non-Gaussian distributions. We choose the following distributions based on physical considerations. To reflect the real experimental setup where the mean of the distribution is subtracted, we standardize the distribution so that all

of them have a zero mean. Furthermore, we normalize the variance of the distribution to be unity. Thus, distributions we study below correspond to the probability distribution functions (PDF) of $x = \frac{\Delta T}{T} \cdot \frac{1}{\sigma_0}$, where σ_0 is the observed rms temperature fluctuations.

1. Exponential distribution.

This distribution may describe the temperature fluctuation produced from the cosmic string network on arcminute scales [11]. The PDF of this distribution is;

$$P(x) = \frac{1}{\sqrt{2}} \exp(-\sqrt{2}|x|). \tag{2}$$

The skewness and kurtosis of the distribution are:

$$\mu_3 = 0; \quad \mu_4 = 1.5. \tag{3}$$

2. Log-normal distribution.

This distribution is widely used in the statistical studies of galaxies and clusters. It is temping to suggest that it might describe the distribution of temperature anisotropy from Sunyaev-Zeldovich (SZ) effects [22]. Since the effect is produced by the hot-gas in the rich clusters, thus it should relate intrinsically to the distribution of rich clusters, which is log-normal. Simulation of SZ in the cold dark matter scenario [23] seems to support this connection. A small reminder is that the SZ effect always produces cold spots on the sky; thus, the distribution of the temperature fluctuation is different from the usual log-normal distribution by a sign. The PDF is given by:

$$P(x) = \frac{1}{\sqrt{2\pi}\sigma(-x)} \exp(-(log(-x))^2/\sigma_2), x < 0. \tag{4}$$

where σ is given by:

$$\sigma = \frac{1}{2} \ln \frac{1+\sqrt{5}}{2}, \tag{5}$$

The skewness and kurtosis of the distribution are:

$$\mu_3 = -\frac{\exp(3\alpha) - 3\exp(\alpha) + 2}{(\exp(\alpha) - 1)^{3/2}}$$

$$\mu_4 = \frac{\exp(6\alpha) - 4\exp(3\alpha) + 6\exp(\alpha) - 3}{(\exp(\alpha) - 1)^2}, \tag{6}$$

where $\alpha = \sigma^2$. Thus,

$$\mu_3 = -0.66, \mu_4 = 2.72. \tag{7}$$

3. χ^2_n distribution.

This class of distributions provides a good fit to the statistics of temperature fluctuation from global topological defects and non-topological defects in the framework of $O(N)$ σ-model [24]. In this model, a global symmetry $O(N)$ is broken to $O(N-1)$ by a N-component real scalar field $\phi = (\phi_1, ..., \phi_N)$ in the early universe. The temperature anisotropy produced by the dynamics of the scalar fields is given by:

$$\frac{\delta T}{T} = -\frac{2\pi G\eta^2}{9}\Theta_{00} = -\frac{2\pi G\eta^2}{9}\sum_i [\dot{\phi_i}^2 + (\nabla\phi_i)^2]. \tag{8}$$

When N is small, the dynamics of the scalar fields are nonlinear, thus, the PDF for ϕ_i is non-Gaussian. However, when N is larger, the dynamical equations for ϕ_i decoupled and become linear [24] and therefore $\phi_i (i = 1, ..., n)$ become independent Gaussians. From Eq. (8), it is clear that in the large N limit, the temperature anisotropy is χ^2 distributed with $n = 4N$ degrees of freedom. Because of our standardization process, the PDF is related to the usual χ^2 distribution by the following transformation:

$$x \to x + \sqrt{n/2}, \quad \sigma^2 \to 1/\sqrt{2n}. \tag{9}$$

Thus, the PDF of the distribution is given by:

$$P(x) = \frac{1}{(2/n)^{n/2}\Gamma(n/2)}(x + \sqrt{n/2})^{\frac{n-2}{2}} \exp(-\frac{\sqrt{2n}\cdot x + n}{2}), x \geq -\sqrt{n/2}. \tag{10}$$

This PDF is plotted in Fig. (1) for $n = 4, 8, 16$. The distribution is very non-Gaussian for low n but approaching asymptotically toward Gaussian in the large n limit. The skewness and kurtosis of the distribution of this class of distribution is:

$$\mu_3 = \sqrt{8/n}, \quad \mu_4 = 15/n. \tag{11}$$

With the presence of Gaussian noise, the skewness and kurtosis will reduce dramatically. While the third and fourth moments of the distribution are unchanged, the variance increases by $(1 + \alpha^2)$, when the signal to noise ratio is $1 : \alpha$. Thus, the skewness will reduce by $(1 + \alpha^2)^{-3/2}$ and the kurtosis

by $(1+\alpha^2)^2$. For the log-normal distribution, the relations mentioned above are not true. The skewness and kurtosis can be calculated from Eq.(6). The skewness and kurtosis for various non-Gaussian distributions are listed in Table 1. In the noisy case, the signal to noise ratio is set to be 1:1.

2.2 Estimate of Skewness and Kurtosis of Noisy Data

In this section, we will address the following questions: how to estimate the skewness and kurtosis from noisy experimental data, and what are the statistics of these quantities when the signal and noise are both Gaussian?

In the case where the experimental data is noisy, one has to deal with two random variables, the signal and the noise, which have a bivariant joint distribution. Thus, we have to generalize the usual skewness and kurtosis to bivariant distributions. Let us first consider the general multivariant distribution. For a $p-$dimensional random vector $\bar{X} = (x_1, x_2, ..., x_p)$ with zero mean and covariance matrix Σ, it is helpful to introduce the following multivariant measures of skewness and kurtosis [25]: For skewness,

$$\beta_{1p} = \sum_{r,s,t=1}^{p} \sum_{r',s',t'=1}^{p} \sigma^{rr'}\sigma^{ss'}\sigma^{tt'}\mu_{111}^{rst}\mu_{111}^{r's't'}, \tag{12}$$

where $\mu_{111}^{rst} =< x_r x_s x_t >$, σ^{ij} is the i,jth element of Σ^{-1}, the inverse of covariant matrix Σ. If the joint-distribution function for $\bar{X}$ is a multivariant Gaussian, then $\beta_{1p} = 0$. β_{1p} can be estimated from a sample of size N, where we can replace the ensemble-averaged μ_{111} and covariance matrix elements with the sample-averaged ones[1]. If we denote the estimate of β_{1p} by b_{1p}, then under the Gaussian hypothesis, the statistic $A = \frac{Nb_{1p}}{6}$ is approximated distributed as a χ^2 with $\frac{p(p+1)(p+2)}{6}$ degrees of freedom. For us, the interesting cases are for $p = 1, 2$. When $p = 1$, $\beta_{11} = \mu_3$, the usual skewness. If one denote b_3 as the estimate of skewness μ_3 from a sample of size N, then

$$b_3 = \frac{1}{N}\sum_{i=1}^{N}\delta_i^3, \tag{13}$$

[1]Here, we explicitly assume that the temperature fluctuation is ergodic so that the ensemble average will be identical to the spatial average (in our case, it is the sample average) in the limit of large spatial coverage. The ergodicity is guaranteed if the power spectrum of the fluctuation is continuous. See Adler [26] and Bardeen, Bond, Kaiser & Szalay [27] for details.

and $A = \frac{Nb_3}{6}$ is distributed as a χ^2 with 1 degree of freedom. For $p = 2$,

$$\beta_{12} = (1-\rho^2)^{-3}\{\gamma_{30}^2 + \gamma_{03}^2 + 3(1+2\rho^2)(\gamma_{12}^2 + \gamma_{21}^2) - 2\rho^3\gamma_{30}\gamma_{03} + 6\rho[(\gamma_{30}\rho\gamma_{12} - \gamma_{21}) + \gamma_{03}(\rho\gamma_{21} - \gamma_{12}) - (2+\rho^2)\gamma_{12}\gamma_{21}]\}, \quad (14)$$

where

$$\rho = \frac{M_{12}}{\sigma_1\sigma_2}, \gamma_{rs} = \frac{\mu_{rs}}{\sigma_1^r\sigma_2^s}, \mu_{rs} = < x_1^r x_2^s > . \quad (15)$$

In the case where signal and noise are both random Gaussian fields, the joint probability distribution function is a bi-variant Gaussian:

$$P(x_1, x_2) = \frac{1}{(2\pi)^2 detM} \exp(-1/2 \sum x_i M_{ij}^{-1} x_j), \quad (16)$$

where the correlation matrix between the signal and noise is the following:

$$M_{11} = \sigma_1^2, M_{22} = \sigma_2^2, M_{12} = M_{21} = < x_1 x_2 > . \quad (17)$$

For COBE DMR, the correlation matrix can be estimated from (A+B)/2 and (A-B)/2 maps. The bi-variant measure of skewness $\beta_{12} = 0$ if we assume that the signal and noise are both Gaussian. Let us denote b_{12} as the estimate of β_{12} from a sample of size N (say, COBE map). Under the Gaussian hypothesis, $A = \frac{Nb_{12}}{6}$ is distributed as a χ^2 with 4 degrees of freedom.

For kurtosis, we have the following measure:

$$\beta_{2p} = [< \bar{X}\Sigma^{-1}\bar{X} >]^2 - p(p+2). \quad (18)$$

Given a random sample of size N on the random vector $\bar{X}$, we can replace the ensemble average with the sample average and estimate β_{22} by

$$b_{2p} = \frac{1}{N}\sum_1^N [(\bar{X}_i - \mu)S^{-1}(\bar{X}_i - \mu)]^2 - p(p+2), \quad (19)$$

where $\mu = \frac{1}{N}\sum_1^N \bar{X}_i$, and $S_{ij} = \frac{1}{N}\sum_1^N (\bar{X}_i - \mu)(\bar{X}_j - \mu)$. For a multivariant Gaussian, $b_{2p} = 0$, and the following statistic $B = [\frac{b_{2p}}{\frac{8p(p+2)}{N}}]^{1/2}$ is approximately distributed as normal with zero mean and variance one.

For p=1, β_{21} reduce to μ_4, the usual kurtosis we defined before. An estimate of μ_4 from a given sample is

$$b_4 = \frac{1}{N}\sum_{i=1}^N x_i^4. \quad (20)$$

and the sample variance is $\sqrt{24/N}$.

For p =2,

$$\beta_{22} = -8 + \{\gamma_{40} + \gamma_{04} + 4\rho(\rho\gamma_{22} - \gamma_{13}\gamma_{31})\}/(1-\rho^2)^2, \qquad (21)$$

where ρ and γ_{rs} is the same as the ones defined in Eq. (15). Under Gaussian assumption, $\beta_{22} = 0$, and the estimation of β_{22}, b_{22} has zero mean and sample variance $\sqrt{48/N}$.

2.3 COBE data

At present, the only existing complete dataset of temperature anisotropies is the COBE dataset. Thus, it is tempting to ultilize the statistics we discussed before and put a constraint on the possible deviations from Gaussianity through COBE data. Unfortunately, the skewness and kurtosis of the distribution of $\frac{\Delta T}{T}$ cannot be estimated directly from the COBE dataset because the signal in each pixel is not an independent measurement of $\frac{\Delta T}{T}$. Furthermore, in order to estimate skewness and kurtosis, we have to assume that the temperature anisotropies are ergodic so that the spatial average is equivalent to the ensemble average. But, even for Gaussian fluctuations, the ergodic hypothesis is true only if the power spectrum of the fluctuations is continuous [26][27]. The observed temperature anisotropies are 2D random fields on a 2-sphere. The power spectra C_l is discretized and asymptotically approaching continuity in the large l limit. For the COBE experiment, which is sensitive only to the low l moments, the ergodic hypothesis doesn't hold. Thus, the statistics estimated from COBE directly will only be the estimates of the "local" values: they are the measure of deviation from Gaussiantiy in our horizon. To estimate the cosmic skewness and kurtosis, i.e., the skewness and kurtosis averaged over an ensemble of horizons, one has to treat the observed value as a N-dimensional random vector, where N is the sample size (the total number of pixels). Since we have only one measurement (we have only one universe), in order to calculate the ensemble average of the quantities equation, the only conceivable way is to use Monte-Carlo simulation. The COBE analysis along this line will soon appear [28] and won't be repeated here. We note that by using the statistics of multivariant skewness, which is a χ^2 distribution with $N(N+1)(N+2)/6$ degrees of freedom. The total number of simulated maps must exceed $N_{map} \geq \frac{N}{\beta_3^2}$, where β_3 is the

variance of the skewness of a distribution. To estimate a skewness with variance smaller than 0.1, the number of simulated maps has to be larger than 6×10^5.

3 Topological Measures of a Random Field

In this section, we will discuss the topological measure of a random field and the application to the test of deviation from Gaussianity. This approach was studied in [29][30]. It is found that among all these quantities, the Euler-Poincare (EP) characteristic is the most effective topological measure with regard to testing Gaussianity. Adler [26] also derived the mean for a special non-Gaussian field: the χ^2 field. Subsequently, Coles [29] applied the result to a number of non-Gaussian fields which are derived from Gaussian. Gott et al. [30] applied EP characteristic to simulated cosmic string maps. Both confirmed that the EP characteristic is effective in testing Gaussianity. We will briefly review the existing results obtained by previous investigators, then we will move on to study the statistics of the topological quantities. Special attention is paid to the real experimental situation where the noise level is high. We also derive some new results on topological measures in the presence of Gaussian noise. We will show that in the case where the signal to noise ratio is around 1:1, the EP characteristic, unfortunately, fails to be effective in discriminating between Gaussian and non-Gaussian distributions.

3.1 Mean

The central concept on which all topological measures are based is the excersion set [26] which is the set of points where the field $F(r)$ exceeds a global value u. If we take a map of a certain area of the CBR sky, the excersion set of the map above level u, denoted by S_u, will in general consist of a number of disjoint regions, each having a boundary which is the contour of satisfying $F(r) = u$. Since the smoothness and the differentiability of the contours are guaranteed by the beam smoothing[2], the Euler-Poincare (EP) characteristic

[2]For noise, without smoothing, the contour will be a fractal and it will not be differentiable. We illustrate this point in Fig. 2. For a detailed discussion, see citeadler, coles.

of S_u, Γ_u is given by:

$$\Gamma_u = \frac{1}{2\pi}\int k ds, \tag{22}$$

where k is the geodesic curvature of the contours and the intergal is taken over all contours in the map.

For Gaussian random fields, the mean of the EP characteristic is exactly calculatable:

$$< \Gamma_\nu >= \frac{1}{(2\pi)^{3/2}}(\frac{C_2}{C_0})^2 \nu \exp(-\nu^2/2), \tag{23}$$

where $C_0 =< T^2(\hat{r}) >$, $C_2 =< \nabla T(\hat{r})\nabla T(\hat{r}) >$ is the variance of the temperature anisotropy gradient[3], and $\nu = u/\sigma$, σ is the rms temperature anisotropy.

Among all possible non-Gaussian PDFs, we specifically choose the χ^2_n distribution because of its relevance to the $O(N)$ σ-model. For our standardized PDF given in Eq. (10), the mean number of the EP characteristic is given by:

$$< \Gamma_\nu >= \frac{1}{4\pi\Gamma(n/2)}(\frac{C_2}{C_0})^2(\frac{\sqrt{n}\nu + n}{2})^{(n-2)/2}(\sqrt{n}\nu + 1)\exp(-(\sqrt{n}\nu + n)/2). \tag{24}$$

3.2 Statistics

The Euler-Poincare characteristic is a discrete point process defined over the underlying random field. For any point process $N(\hat{r})$ with mean $< N >= \bar{N}$, the variance of the process is given by [31]:

$$< N^2 >= |\bar{N}| + \bar{N}^2(1 + \bar{\xi}), \tag{25}$$

where

$$\bar{\xi} = \frac{1}{A^2}\int d\Omega_1 d\Omega_2 \xi(\hat{r}_{12}) \tag{26}$$

is the sample-area averaged two point correlation of the process N. The first term in Eq. (25) is due to the discreteness of the process. The variance of the process is given by:

$$\sigma^2 =< N^2 > -\bar{N}^2 = \bar{N} + \bar{N}^2\bar{\xi}. \tag{27}$$

[3] C_2/C_0 is equal to $\sqrt{2}\gamma^2/\theta_*^2$, where γ and θ_* is the spectral parameters defined by [12].

Thus, to find the variance of the EP characteristics, the central problem is to find the two point correlation. We approximate this correlation function ξ by the peak-peak correlation χ of the same underlying random field. Since $\Gamma(\nu)$ is defined through the ν-peaks of the density field, the approximation should provide a reasonable fit to the true Γ correlation. We expect that this approximation will give poor results when $\Gamma(\nu) \sim 0$.

The peak-peak correlation function is well studied in the literature [32] [12] and is most easily understood as the following: Let $P_1(\hat{r})$ be the probability of finding one $\nu-$peak at $\hat{r}$ and P_2 be the probability of finding a $\nu-$peak at $\hat{r}_1$ and $\hat{r}_2$. Then, the two point correlation for the peaks will be:

$$1 + C_2(\hat{r}_1, \hat{r}_2) = P_2/P_1^2. \tag{28}$$

For a Gaussian random field, we have

$$P_1 = \frac{1}{\sqrt{2\pi}\sigma_0} \int_{\nu\sigma_0}^{\infty} dx \exp(-\frac{x^2}{2\sigma_0^2}), \tag{29}$$

and

$$P_2 = \frac{1}{2\pi \det M} \int_{\nu\sigma_0}^{\infty} \int_{\nu\sigma_0}^{\infty} dx_1 dx_2 \exp(-\frac{1}{2}\bar{\mathrm{x}} M^{-1} \mathrm{x}), \tag{30}$$

where $\mathrm{x} = (\mathrm{x}_1, \mathrm{x}_2)$ and $M(r_1, r_2)$ is the correlation matrix of the random field at r_1, r_2, which is

$$M = \begin{vmatrix} 1 & \psi(\theta) \\ \psi(\theta) & 1 \end{vmatrix} \cdot \sigma_0 \tag{31}$$

and $\psi(\theta)$ is the normalized two point function. Thus, in the limit where $\psi \ll 1$, the peak-peak correlation function is given by:

$$\xi_{peak} = \nu^2 \psi(\hat{r}). \tag{32}$$

The beam-smoothed two point temperature correlation is well approximated by :

$$C(\theta) = C(0) \exp(-\theta^2/\theta_c^2), \tag{33}$$

where the coherent angle $\theta_c \approx \theta_*$, is a function of the beam width. The averaged correlation in an area $A = \pi\theta_A^2$ is

$$\bar{\psi} = \nu^2 (\frac{\theta_c}{\theta_A})^2. \tag{34}$$

Thus, the variance of the Euler-Poincare characteristic is given by:

$$\sigma^2 = |\bar{N}| + \nu^2(\frac{\theta_c}{\theta_A})^2\bar{N}^2, \bar{N} = n(\pi\theta_A^2). \tag{35}$$

The mean and 1σ uncertainty of the EP characteristic $\Gamma(\nu)$ for Gaussian random field is plotted in Fig. 3. Because of the approximations we used to derive the statistic, we expect the uncertainties of $\Gamma(\nu)$ given by Eq. (35) are not exact when $\nu \sim 0$.

3.3 The EP Characteristic of Noisy Data

Our major concern over the applicability of the EP characteristic as a reliable statistic to discriminate between a Gaussian and a non-Gaussian random field is the noise term, which appears in all current CBR experiments and is comparable in amplitude to the signal. In this section, we will show first how the beam used in the experiments regulates the noise. Without smoothing, noise will be an obvious hazard to topological measures because the rms of the derivatives of noise is not well defined. We will then proceed to study the change of EP characteristic due to the beam-smoothed noise term.

The spectral parameter of the noise is given by:

$$\sigma_0^2 = A\sum_{l=2}(2l+1)\exp(-l(l+1)\sigma_s^2) \sim A(\frac{1}{\sigma_s})^2, \tag{36}$$

$$\sigma_1^2 = A\sum_{l=2} l(l+1)(2l+1)\exp(-l(l+1)\sigma_s^2) \sim \frac{1}{2}A(\frac{1}{\sigma_s})^4 \tag{37}$$

$$\sigma_2^2 = A\sum_{l=2}(l-1)l(l+1)(l+2)(2l+1)\exp(-l(l+1)\sigma_s^2) \sim \frac{1}{3}A(\frac{1}{\sigma_s})^6. \tag{38}$$

Thus, $\gamma = \frac{\sigma_1^2}{\sigma_0\sigma_2} = 0.75$ and $\theta_* = \sqrt{2}\frac{\sigma_1}{\sigma_2} = \sqrt{3}\sigma_s$. If we compare this value for noise with that of a Harrison-Zeldovich primordial perturbation, where $\gamma \sim 0.5$ and $\theta_* \sim 1.8\sigma$, we can conclude that the noise term regulated fairly well by the beam.

However, even with a beam-smoothing, the EP characteristic of the observed random temperature anisotropy pattern is still changed due the presence of noise. We first consider a situation where the sky is dominated by a quadrupole only, as we showed Fig. (4a). The EP characteristic is very

simple for this map: $\Gamma = 2$ for $\nu = -1, 1, 2$. However, when one puts Gaussian noise of the same variance to the signal, the map is dominated by the feature of noise, which are shown in Fig. (4b). Even though we don't expect the temperature anisotropies to be a pure quadrupole, this example makes us cautious when using the EP characteristic. In the realistic cases where the signal itself is also a random field which is non-Gaussian, the problem is harder. A full analysis of the EP characteristic for the sum of two general random fields is not tractable. Only one special case where both fields are Gaussian is solved [26]. In our problem, where one field is non-Gaussian, there is no ready-to-use result to apply. Thus, we solve this problem by the following strategy: the $\chi^2_n, n = 1, ...$ is a class of distributions, ranging from very non-Gaussian (small n) to slightly deviating from Gaussian (large n), and the EP characteristic of this class of distribution is known. Thus, we first find the modified non-Gaussian PDF due to the presence of noise, then we find the best fit χ^2 distribution to this modified PDF. The EP characteristic of the noisy temperature map is thus approximated to be the EP characteristic of the best fit χ^2 distribution. The validity of this approach lies partly in the fact that if the difference between two PDFs goes to zero, the difference between the corresponding EP characteristic also goes to zero.

We assume the noise is Gaussian and uncorrelated with the CBR anisotropy signals. The PDF for the noise is:

$$P(\eta) = \frac{1}{\sqrt{2\pi}\sigma_n} \exp(-\eta^2/2\sigma_n^2) \tag{39}$$

where σ_n is the variance of noise. In the following, we consider only the case where the signal to noise ratio is 1:1, thus $\sigma_{noise} = \sigma_{signal} = 1/\sqrt{2}$. It is straightforward to generalize to the arbitrary noise case, and we will show it here.

The PDF for the noisy map is given by:

$$P(x) = \int P_{\rm signal}(x') P_{\rm noise}(x - x') dx' \tag{40}$$

It is convenient to use the cumulant function [33] $K(u)$, which is the logarithm of the characteristic function $\phi(u)$, the Fourier transformation of the PDF:

$$\phi(u) = \int P(x) e^{iux} dx. \tag{41}$$

The cumulant function for $P(x)$ is simply the sum of the cumulant function of the signal and the noise. For Gaussian noise, the cumulant function is simple: $K_{noise}(u) = -\frac{u^2}{4}$. For the signal, the PDF is the modified χ^2 distribution. After some algebra, the cumulant is found to be:

$$K_{signal}(u) = \frac{n}{2}\ln(1 - \frac{iu}{\sqrt{n}}) + i\sqrt{n}u/2. \tag{42}$$

Thus, the cumulant function for the noisy signal is given by:

$$K(u) = K_{noise}(u) + K_{signal}(u) \approx -u^2/2 + \frac{i}{6\sqrt{n}}(\frac{u}{\sqrt{2}})^3, \quad \mathrm{n} \gg 1 \tag{43}$$

Thus, with noise, the cumulant is still that of a χ^2 distribution in the limit of large n, but with N degrees of freedom, where $N = 2^{3/4}n \sim 1.7n$. In Fig. 5, we plot the EP characteristic for $n = 12$ with and without noise. Even for the global monopole where $n \simeq 12$, the EP characteristic fails to be effective.

4 Three Point Temperature Correlation Function

There are various examples where non-Gaussian processes possess Gaussian PDF [18]. One classic example is the smoothed Poisson point process. The process is non-Gaussian when the smoothing scale is small, and tends to be Gaussian when the smoothing scale becomes large by the virtue of the central limit theorem [19]. Thus, the test of Gaussianity should go beyond the mere one point PDF. The EP characteristic discussed in the previous section is one way to take into account the full properties of a random Gaussian field. But the noise present in the data prevents it from being effective. However, as we stressed before [15], the three point temperature correlation function is a good measure of deviations from Gaussianity for the noisy data, as long as the noise is mutually independent and not correlated with signals. In this section, we will first introduce statistics to test these aspects of noise. Then, we will discuss theoretical predictions of the three point function in different models [34]. The reduced three-point functions for COBE 53 GHz signal and noise maps are obtained and show no deviation from Gaussian. We conclude that at the COBE scale, the temperature anisotropies are probably Gaussian.

4.1 Properties of Noise

A good understanding of noise in CBR experiments is crucial in testing the Gaussianity of the primordial density perturbation through the existing data. One has to make specific assumptions about the instrumental noise in order to test the Gaussianity: the instrumental noise must be mutually independent among pixels and Gaussian. The assumption has to be tested thoroughly before any attempt to decipher the non-Gaussian CBR signal from the data. The statistical tools of testing Gaussianity we introduced throughout this paper should also apply to the noise and we wouldn't repeat them here. In this section, we will address the following aspects related to the noise in the experimental data: (1) is the noise mutually independent? (2) does noise correlate with the CBR signals?

In testing the mutual independence of the noise, we use the following results from statistics [25]: Let $y_i, (i = 1, ..., N)$ be a measurement of a zero mean random process. The mean and two point correlation of the process can be estimated as the following:

$$\bar{y} = \frac{1}{N}\sum_{i=1}^{N} y_i, \tag{44}$$

$$C_2(s) = \frac{1}{N}\sum_{i=1}^{N-|s|}(y_i - \bar{y})(y_{i+|s|} - \bar{y}), s = 0, \pm 1; ..., \pm(N-1), \tag{45}$$

$$\rho(s) = C_2(s)/C_2(0). \tag{46}$$

Then, if y_i are mutually independent, then $\rho(s)$ is asymptotically Gaussian. In particular, $\rho(1)$ is asymptotically Gaussian with zero mean and variance $\frac{1}{N}$. With a suitable redefinition of y_i, this result can be applied to answer questions (1) and (2).

(1)Testing for the Independence of the Noise

Let $\eta_i, i = 1, ..., N$, be the noise in ith pixel. The mutual independence of noise can be tested through a second covariance of analysis of the square of the noise. Let $y_i = \eta_i^2, i = 1, ..., N$. If η_i are not correlated, then y_i will not be either. Thus, we can define the following statistic:

$$W_n = \frac{\rho(1)C_2(0)\sqrt{N}}{\sqrt{C_4(0,1,1)}}, \tag{47}$$

where

$$C_4(0,1,1) = \frac{1}{N}\sum_{i=1}^{N-1}(y_i - \bar{y})^2(y_{i+1} - \bar{y})^2. \tag{48}$$

Under the hypothesis that the noise are independent, W_n is distributed as a standard Gaussian (zero mean and unity variance). We can define W_s, the same statistic as W_n by using the signal in each pixel, to test the independence of the signal.

(2) Testing the Correlation among Signal and Noise

Noise should not only be uncorrelated, but should also be independent of the signal. We assume that the noise is additive, i.e., $\delta_{obs} = \delta_{CBR} + \eta$. Once the noise is found to be independent, the variable

$$y_i = \eta_i^2 \delta_i^{obs} = \eta_i^2(\delta_i + \eta_i), \tag{49}$$

should also be mutually independent. Following the previous section, the following set of statistics

$$W_c = \frac{\rho(1)C_2(0)\sqrt{N}}{\sqrt{C_4(0,1,1)}}, \tag{50}$$

with

$$C_4(0,1,1) = \frac{1}{N}\sum_{i=1}^{N-1}(y_i - \bar{y})^2(y_{i+1} - \bar{y})^2, \tag{51}$$

is a standard Gaussian.

(3) Analysis of COBE GHz DMR Map

For COBE DMR, the (A+B)/2 is the signal+noise map and the (A-B)/2 is the noise map. The properties of signal and noise are tested through the statistics defined aboved and shown in Table 2.

The analysis shows that at the 1.6% confidence level, the noise is uncorrelated. At the 19% confidence level, the noise is not correlated with the signal. Thus, we can conclude that the noise in COBE 53 GHz map is not correlated with the signal and marginally uncorrelated. The W_s in the last row is the statistic to test the independence of the signal. The statistic shows that the hypothesis that the data is not correlated failed badly. This is expected if the signal is primordial CBR fluctuations.

4.2 Three Point Function

It is convenient to use the normalized two point ψ and three point function η, where

$$\psi(|\hat{r}_1 - \hat{r}_2|) = C_2(\hat{r}_1, \hat{r}_2)/C_2(0), \quad \psi(0) = 1 \tag{52}$$

$$\eta(\hat{r}_1, \hat{r}_2, \hat{r}_3) = < \frac{\delta T}{T}(\hat{r}_1)\frac{\delta T}{T}(\hat{r}_2)\frac{\delta T}{T}(\hat{r}_3) > /C_2(0)^{1.5}, \quad \eta(0) = \mu_3, \tag{53}$$

where μ_3 is the skewness. The theoretical predictions for three point function are mainly the following:

(1) Inflation

Various non-standard inflation models [5] will generate a non-zero three point correlation function. The generic form of the three point function in most inflationary models is:

$$\eta(\hat{r}_1, \hat{r}_2, \hat{r}_3) = \frac{\lambda}{3}(\psi(|\hat{r}_1 - \hat{r}_2|)\psi(|\hat{r}_1 - \hat{r}_3|) +$$
$$\psi(|\hat{r}_1 - \hat{r}_2|)\psi(|\hat{r}_2 - \hat{r}_3|) + \psi(|\hat{r}_1 - \hat{r}_3|)\psi(|\hat{r}_2 - \hat{r}_3|)), \tag{54}$$

where λ is a dimensionless constant. As we will show in the Appendix, for one field slow-roll inflation models, $\lambda \sim 10^{-7}$. In non-standard inflation models [5], σ can be much larger (up to order unity).

(2) χ^2 fields.

Consider the χ^2 field $Y = \sum_{i=1}^{n} X_i^2$. As we discussed before, the χ^2 field describes the global topological defects in the large N limit. By extrapolating to low N, one can also gain insights into the possible temperature anisotropy patterns generated by domain walls, strings, monopoles or textures. The two point correlation is given by:

$$C_2(\hat{r}_1, \hat{r}_2) = 2n\phi^2(\hat{r}_1, \hat{r}_2), \tag{55}$$

where ϕ is the common covariance function of the X_i. We choose ϕ so that the two point function of Y matchs the observation,

$$\phi^2(\hat{r}_1, \hat{r}_2) = C_2(\hat{r}_1, \hat{r}_2)/2n. \tag{56}$$

The three point function is found to be:

$$\eta(\hat{r}_1, \hat{r}_2, \hat{r}_3) = \sqrt{8/n}(\psi(|\hat{r}_1 - \hat{r}_2|)\psi(|\hat{r}_1 - \hat{r}_3|)\psi(|\hat{r}_2 - \hat{r}_3|))^{3/2} \tag{57}$$

(3) Late-time Phase Transition

In this model [35], due to the conformal invariance of the system at the critical point [36], the three point function result from this class of cosmological phase transitions has the following simple form:

$$\eta(\hat{r}_1, \hat{r}_2, \hat{r}_3) = \alpha(\psi(|\hat{r}_1 - \hat{r}_2|)\psi(|\hat{r}_1 - \hat{r}_3|)\psi(|\hat{r}_2 - \hat{r}_3|))^3, \quad (58)$$

where α is a dimensionless constant of order unity.

The full structure of η is complicated. We consider the reduced three point function[37] where

$$\eta_{reduced}(\hat{r}_1, \hat{r}_2) = < (\frac{\delta T}{T})^2(\hat{r}_1)\frac{\delta T}{T}(\hat{r}_2) > /C_2(0)^{3/2}. \quad (59)$$

The theoretical predictions in various models are given by:

$$\eta_{reduced}(\hat{r}_1, \hat{r}_2) = \frac{\mu_3}{3}(1 + 2\psi(|\hat{r}_1 - \hat{r}_2|)) \text{ for inflationary models} \quad (60)$$

$$\eta_{reduced} = \sqrt{2/N}\psi^3(|\hat{r}_1 - \hat{r}_2|) \text{ for O(N)}\sigma - \text{models} \quad (61)$$

$$\eta_{reduced} = \alpha\psi^6(|\hat{r}_1 - \hat{r}_2|) \text{ for LTPT models} \quad (62)$$

The three point functions from the previous three different categories are plotted in Fig. 6, the skewness is chosen to be the same for all cases.

4.3 Analysis of COBE data

The 53 GHz COBE DMR data is analyzed ultilizing the statistics we discussed above. This frequency (53 GHz) is chosen because it has the best data quality [8]. Before subtracting the dipole and beginning further analysis, the signal is weighted by the estimated pixel uncertainty. The dipole is subtracted by using the most recent COBE result [38]. For 53 GHz (A+B)/2 map, the subtracted dipole signal is:

$$T(l, b)(mK) = -0.198 \cdot \cos(l)\cos(b) - 2.075 \cdot \sin(l)\cos(b) + 2.333 \cdot \sin(b), \quad (63)$$

where l and b are the galactic longitude and latitude. In our analysis, we consider only the 2019 pixels whose galactic latitude is 20 degrees or above. The COBE 53 GHz (A+B)/2 and (A-B)/2 are analyzed and the reduced three-point functions are shown in Fig. 7a, 7b. The result is consistent with Gaussian fluctuations and there is no deviation above the statistical uncertainty. We conclude that the current analysis shows that the statistics of CBR at the COBE scale are probably Gaussian.

5 Statistical Tests on Intermediate Angular Scales ($\theta \sim 1^\circ$)

The Gaussianity question is hard to resolve on the COBE scale ($\theta \sim 7^\circ$) even if there is no noise in the experimental data. One should expect the CBR on the large angular scale to be Gaussian simply by virtue of the central limit theorem [19]. Furthermore, there is intrinsic uncertainty in the statistical quantities measured in our local universe due to the cosmic variance [39], which makes it harder to discriminate between Gaussian and non-Gaussian fluctuations on the COBE scale alone. On intermediate angular scales ($\theta \sim 1^\circ$), the cosmic variance is small and the chance to detect a non-Gaussian signal is higher. As the data on these scales is accumulating, it is timely to consider seriously testing Gaussianity on these scales, since data in some experiments [40][41] show clear non-Gaussian features. Although the current experiments are inclusive, due to the possible foreground contamination, it gives us hope that the Gaussianity problem will be resolved experimentally in the near future. The EP characteristic and the three point correlation will apply equally on both large and small angular scales if the sky coverage of the experiment is substantial. However, as the current state-of-the-art intermediate scale CBR experiments cover a tiny fraction of the sky, more sophisticated statistical tools [14] are required to carry out the tests. In this section, we will introduce and discuss the bispectral analysis and the Hotelling's T^2 statistic. We will show that the T^2 statistic is a powerful statistical quantity to use on these scales and we also estimate the minimun data sample size to carry out the Gaussian test through T^2 statistic.

In most current intermediate scale experiments, the data is sampled either in thin long strips or an annulus around an axis. In both cases, the data is one dimensional. The three-point function and bispectral analysis of 1-d data are well studied by statisticians and much of the specific techniques and mathematical details of this section are contained in monographs by [25][42] which interested readers should consult. One can arrange the dataset as a time series, X_t, where in the present case, "time" t refer to successive positions in the sky. The data is usually edited so that the mean is removed.

In this case, the three-point function is simply

$$\xi_{t_1,t_2} =< X_t X_{t+t_1} X_{t+t_2} >_t = \frac{1}{N}\sum_{i=1}^{N} X_i X_{i+t_1} X_{i+t_2}, \tag{64}$$

where the expression on the left-hand side is an estimate of three point function from a data sample and N is the size of the sample. Since the temperature anisotropies are always real-valued and assumed to be homogeneous and isotropic, the three point function has the following symmetry:

$$\xi_{t_1,t_2} = \xi_{t_2,t_1} = \xi_{-t_1,t_2-t_1} = \xi_{t_1-t_2,-t_2} \tag{65}$$

The bispectral density $f(\omega_1,\omega_2)$ is the Fourier transformation of ξ_{t_1,t_2}, where

$$f(\omega_1,\omega_2) = \frac{1}{(2\pi)^2}\int dt_1 dt_2 e^{-it_1\omega_1 - it_2\omega_2}\xi_{t_1,t_2}; \quad -\pi \le \omega_1,\omega_2 \le \pi. \tag{66}$$

In general, $f(\omega_1,\omega_2)$ is a complex function, following the symmetry of ξ, one obtains the following symmetry relation for f:

$$f(\omega_1,\omega_2) = f(\omega_1,\omega_1-\omega_2) = f(-\omega_1-\omega_2,\omega_2) = f^*(-\omega_1,-\omega_2) \tag{67}$$

Because of the symmetry, one just has to estimate the bispectral density in a small portion of (ω_1,ω_2) parameter space.

The unique feature of the Gaussian process is that the bispectral density vanishes for all ω, i.e., $f(\omega_1,\omega_2) = 0$ for all ω_1,ω_2. To test this hypothesis, one can use the Hotelling's T^2 statistics[25], which is constructed from the bispectral estimates defined on a "coarse-grained" frequency grid, (ω_i,ω_j), where

$$\omega_i = \frac{i\pi}{K}, \omega_j = \frac{j\pi}{K}, i = 1,2,...,L; \quad j = i+1,...,\gamma(i), \tag{68}$$

where $L = [\frac{2K}{3}]$, $\gamma(i) = K - [\frac{i}{2}] - 1$. The parameter K is chosen to be much smaller than the sample size so that the frequency grid is "coarse-grained". Let $\eta_{ij} = f(\omega_i,\omega_j)$ and rearrange η_{ij} into a vector $\eta = (\chi_1,...,\chi_P)$, where $P = \sum_{i=1}^{L}(\gamma(i) - i)$ so that for each $l, 1 \le l \le P$, $\chi_l = \eta_{ij}$.

To estimate the bispectral density at each "coarse" grid point, one can construct a "fine" frequency grid around each (ω_i,ω_j) point. Specifically,

$$\omega_{i_p} = \omega_i + \frac{pD\pi}{N}, p = -r, -r+1, ..., r$$
$$\omega_{i_q} = \omega_i + \frac{qD\pi}{N}, q = -r, -r+1, ..., r, (q \neq 0) \tag{69}$$

where the distance D is chosen so that the bispectral estimates at neighboring points on this fine grid are approximately uncorrelated. To insure that points in different "fine" grids don't overlap, it is required that $D \leq \frac{N}{K(2r+1)}$. Since the total number of points in each "fine" grid is $(4r+1)$ and there are $K^2/3$ "coarse-grained" grids, thus the constraint on parameter r is: $(4r+1)K^2/3 < N$.

Let $\hat{f}(\omega_{i_p}, \omega_{i_q})$ denote the estimated bispectral density function at the points $(\omega_{i_p}, \omega_{i_q})$. Due to the careful choice of grid point, one may regard the set of estimators $\{\hat{f}(\omega_{i_p}, \omega_{i_q})\}$ as $n = 4r+1$ uncorrelated and unbiased estimates of $f(\omega_i, \omega_j)$. Forming the bispectral estimates $\hat{f}(\omega_{i_p}, \omega_{i_q})$ into a n column vector, denoted by $\xi = (\xi_1, \xi_2, ..., \xi_n)$, then, at each "coarse-grained" grid point χ_l, there will be an estimated bispectral density $\xi_i^{(l)}$ from the "fine-grid". When the sample size N is large, $\xi_i^{(l)} (i = 1, 2, ..., n)$, is distributed as complex normal with mean η and covariance matrix Σ_ξ. The maximum likelihood estimates of η and Σ_ξ are:

$$\hat{\eta} = \frac{1}{n}\sum_{i=1}^{n} \xi_i^{(l)}, \quad \hat{\Sigma} = \frac{A}{n}, \quad A_{ij} = \sum_{k=1}^{n} ((\xi_{ik} - \eta)(\xi_{jk} - \eta)^*). \tag{70}$$

The Hotelling's T^2 statistics are defined as:

$$T^2 = n\hat{\eta} A^{-1} \hat{\eta}. \tag{71}$$

Under the Gaussian assumption, the mean vector $\eta = 0$ and the statistic

$$F = \frac{2(n-P)}{2P} T^2 \tag{72}$$

is distributed as a central F-distribution with (2P, 2(n-P)) degrees of freedom.

To test Gaussianity through degree scale experiments, the sample size should be large enough to avoid "sample variance" [43]. The minimal sample size that could be used to carry out the Gaussian statistical tests can be estimated as follows: to carry out the bispectral analysis and Hotelling's T^2 statistics, one should use at least two "coarse" grids, and because the correlation angle of the beam-smoothed CBR anisotropies is around θ_*, where $\theta_* \simeq 1.8\theta_s$ for Harrison-Zeldovich primordial spectrum [12]. Thus, we need at least two "fine" grids on either side of the "coarse" grid. The minimum parameters to test Gaussianity is $L \geq 2$ and $r \geq 2$, which in turn gives

$K \geq 4$. Thus, the minimum sample size is: $N \geq (4r+1)K^2/3 = 48$. This is about twice the current largest sample at the half degree scale [44]. This result is encouraging: it suggests that we don't need a full sky coverage with half-degree resolution to carry out the Gaussianity test, and the Gaussianity question can be resolved by ground-based experiments or balloon flights. With regard to sampling in the sky, the data should sample as sparsely as possible to avoid possible correlation between different data points, and it will be better to sample in thin long stripes or annuli to take advantage of the simplicity of one dimensional dataset. Currently, most degree scale experiments have fewer data points and are thus inadequate to perform bispectral analysis. However, we expect the situation will change dramatically soon, and the results we discuss here will be helpful for designing future experiments.

6 Gaussianity of CBR on Small Scales

In this section, We will show how to use the T^2 statistic by analyzing the recent 96 point RING data from OVRO [20]. A special class of non-Gaussian signal, point sources, which are interesting in their own right, is separated out and discussed in detail in the next section. The data sample is weighted according to the error in each pixel. The sample size $N = 96$. The estimate of the three-point function is shown is Fig. 8a and the the real and imaginary part the bispectrum is shown in Fig. 8b, 8c. We have used an optimum window function (see [25] for details) to smooth the discrete data. For Gaussian distributed data, both the three-point function and bispectrum should vanish. The results shown in Fig. 8a, 8b, 8c already suggest that the data might be non-Gaussianly distributed. To show how statistically significant the deviation from Gaussian distribution, we can use the Hotelling's T^2 statistics. The parameters we choose for RING data are: $K = 4, r = 2, n = 9, d = 4, P = 2, L = 2$. With this choice of parameters, the statistical distribution for F is shown in Fig. 9. The 95% confidence level (C.L.) upper limit of F is $F_c = 3.15$ if the data are Gaussian distributed. Hotelling's T^2 statistic estimated from RING data is $T^2 = 5.76$, or $F = 7T^2/2 = 20.1$ which is much larger than the 95% C.L. upper limits for Gaussian distributions. Thus, we conclude that the data are probably not consistent with Gaussian statistics.

Even though the data failed the statistical tests we proposed, one cannot conclude that the non-Gaussianity is due to non-trivial interactions in the inflationary cosmology or the topological defects produced in the early universe. The non-linear gravitational evolution will produce non-Gaussian signals which have to be carefully studied and subtracted to gain some knowledge about the Gaussianity of primordial perturbations. Part of the answer to this important issue is contained in the next section and we will not discuss here.

7 Point Sources

On intermediate angular scales ($\sim 1^\circ$), the current datasets are too small to carry out the three-point correlation and the angular bispectrum analyses we developed in the previous sections. To test Gaussianity based on the small dataset available (usually about 10 data points), the statistics have to be very custom-designed to be useful [14]. However, a clear non-Gaussian signature will be the point-like CBR anisotropies. In fact, two candidates of such sources are detected in the MSAM experiment [40]. One source, located in a dust-free region, has a flux of 3.7 ± 0.9Jy at 5.6cm^{-1}. Another candidate, has a flux of 2.9 ± 0.7Jy, is located 4.3° away from the first sources. Both sources are compact and have angular size less than the beam width $\sigma = 0.425\theta_{FWHM} = 12'$. Assuming that the angular size of the sources are half the beam width, one can find the the flux intensities are $(3.8 \pm 0.8) \times 10^5 \text{JySr}^{-1}$ and $(3 \pm 0.6) \times 10^5 \text{JySr}^{-1}$. As a comparison, the flux of a δT temperature fluctuation will produce a flux

$$I_\nu = B_\nu(T_0) \frac{\exp(h\nu/kT_0)}{\exp(h\nu/kT_0) - 1} \left(\frac{h\nu}{kT_0}\right) \frac{\delta T}{T_0}, \tag{73}$$

where $T_0 = 2.73K$ is the CBR temperature and B_ν is the CBR flux at frequency ν. At 5.6 cm^{-1}, the CBR flux is $B_\nu = 1.5 \times 10^9 \text{JySr}^{-1}$. Thus, for a temperature anisotropy of $40\mu K$, which is the theoretically estimated temperature anisotropy at the half degree angular scales for CDM with standard recombination [45], the expected flux is

$$I_\nu = 6.8 \times 10^4 \left(\frac{\delta T}{40\mu K}\right) \text{JySr}^{-1}. \tag{74}$$

Thus, the first sources correspond to a 5σ and the second sources correspond to a 4σ peak.

In the Gaussian picture, for a $\nu-$peak, the mean size $\bar{\theta}$ and the average distance between peaks $\bar{d}$ are given by [12]:

$$\bar{\theta} \sim \sqrt{2}\frac{\theta_*}{\gamma\nu}\sqrt{1-\frac{1}{\nu^2}}, \quad \text{for} \quad \nu \gg 1, \tag{75}$$

$$\bar{d} = 2/3(\pi n_\nu)^{-1/2}, \tag{76}$$

where $\theta_* = 1.2\theta_s$ and n_ν is the number density of ν peaks. For large ν, n_ν is given by:

$$n_\nu = \frac{\gamma^2(\nu^2-1)}{(2\pi)^{3/2}}\exp(-\nu^2/2). \tag{77}$$

Thus, for 4σ peaks, the mean size will be $0.71\theta_*$, which is marginally consistent with observation, but the the mean distance between rare peaks will be: $\sim 50\theta_s \sim 20°$, which is much larger than the angular separation between the sources. One may try to explain both point sources by Gaussian statistics, assuming that they are just 3 σ peaks and fit the low limit of the observed flux. Then the average distance between peaks is $11\theta_s$, which is roughly the same as the observed value. However, in this case, the averaged angular sizes of the peaks are $1.2\theta_s$, which is larger than the beam width. We conclude that if these sources are of CBR origin, they are not consistent with Gaussian statistics.

Various topological defects, notably soft domain wall bubbles [46], the global monopoles [47] or textures [24], are capable of producing spot-like CBR anisotropies of any size by appropriately choosing model parameters. However, before one relies on topological defects as an answer, one has to filter out the foreground contaminations carefully. Several types of radiation may contribute the point-like sources observed in the experiments. One of them is the Sunyaev-Zeldovich (SZ) effect from rich clusters. The scattering of microwave photons by hot electrons in the intracluster gas will make a cluster a powerful source of submillimeter radiation. The typical angular size of the core of the hot gas is of order arcminutes, and the flux density is given by [22]:

$$F_\nu = y(x\frac{e^x+1}{e^x-1}-4)\cdot\frac{xe^x}{e^x-1}\cdot B_\nu(T_0), \tag{78}$$

where $x = \frac{h\nu}{kT_0}$ and $y = \int \frac{kT_e}{m_e c^2}\sigma_T n_e dl$. For a typical rich cluster, $T_e \sim 10^7 K$, $n_e \sim 10^{-3}\text{cm}^{-3}$ and $l \sim 1\text{Mpc}$, the estimated y parameter is around $10^{-4} - 10^{-5}$, The flux density is around $3 \times 10^5 \text{JySr}^{-1}$ which is exactly what the MSAM experiment observed. Thus, it is very likely that the observed sources are due to SZ effects of unresolved rich clusters in the field.

The multifrequency channel methods is widely used to separate the local contamination from true CBR signals. The method may not be effective to single out the SZ effect. As we showed in Fig. 10, the spectral index of the SZ effect is very close to that of primordial temperature fluctuations at low frequencies ($\nu < 100$ GHz). When the frequency gets higher ($\nu > 200$ GHz), there is a small deviation, but at this frequency range, the dust emission will dominate. A possible way to discriminate the SZ effect is through polarization of the radiation from candidate point sources. Due to the peculiar velocity of the rich clusters, the radiation will be polarized in SZ effect [22]. However, the point-like CBR anisotropies from topological defects will not. But since it is currently hard to measure the polarization of the radiation down to required accuracy, we won't discuss this approach in detail here.

Apart from the SZ effect, primeval dust [48] or a population of IRAS-like galaxies at high redshift [49] may have substantial contributions at the submillimeter range. For dust grains, if one assumes the emissivity of the dust is $\sim \nu^\alpha, \alpha \approx 1.5$, the flux spectrum of dust emission is given by:

$$f_\nu \sim (\frac{h\nu}{kT_d})^{4+\alpha}\frac{1}{\nu}\frac{1}{e^{\frac{h\nu}{kT_d}} - 1}. \tag{79}$$

The peak of the distribution is located at

$$\nu_{pk} = 4.5kT_d/h = 3750\text{GHz}(T_d/40K). \tag{80}$$

Thus, in order for the peak of a hot dust spectrum ($T_d = 40K$) to be redshifted into the 300 GHz range which the MSAM experiments operates, the redshift of the epoch of formation of primeval galaxies should be around $z \sim 10$. The angular size of the dust envelope is

$$\theta = \frac{l(1+z)}{D}, \quad D = 2H_0^{-1}(1 - \frac{1}{\sqrt{1+z}}), \tag{81}$$

where l is the proper size of the dust envelope, which is about $10 - 100$ kpc. Thus the typical angular size of the possible point sources produced by the

primeval galaxies is

$$\theta = 0.03' \frac{l}{10\text{kpc}} \quad \frac{1+z}{10} \quad (\frac{h}{0.5})^2. \tag{82}$$

The observed flux density is

$$S_\nu = \frac{L(\nu_1)}{4\pi D^2(1+z)}, \nu_1 = (1+z)\nu. \tag{83}$$

Assuming that, in the rest frame of the sources, the intrinsic flux is peaked around 3000 GHz and the luminosity is L, then the flux density is

$$S_\nu = 10^{-3}\text{JySr}^{-1}(\frac{L}{10^{13}L_\odot})(\frac{10}{1+z})(\frac{3000\text{GHz}}{\nu}) \tag{84}$$

Both the angular size and the flux density are too small to account for the observed flux in the MSAM experiment [40]. Thus we can conclude that primeval dust or the distant infrared galaxies do not account for the point-like sources observed.

As we showed in Fig. 11, which is plotted according to Eq. (79), it is clear that if there is a population of cold dust ($T_d \sim 4K$), then the flux density will peak near where the experiment operates. A uniform background of such cold dust is impossible unless the density the low enough so that the optical light from distant quasars will not be absorbed. However, clumpy cold dust is helpful to explain the experimentally observed point-like sources. A possible scenario to explain the spot-sources based on cold dust is the following: there is a population of very quiet galaxies where most of the star formation activities are shut down, so that there will be very low intensity radiation in the far-infrared regime. Thus, this population of galaxies is not observed by the IRAS flux limited survey. However, as the hot dust cools down to around 4K, they become powerful submillimeter emitters. The spectrum of cold dust emission is shown Fig. 11. Multi-spectral analyses can shed light on the possible spectral parameter of the sources. The problem with the cold dust scenario is that as one look back in time, these sources used to be very powerful infrared sources because the radiated flux $\propto T_d^{4+\alpha}$. Due to the abundance one observes today, we can estimate the luminosity at high redshift, which is much brighter. However, the newest result from the COBE FIRAS [50] has already put a stringent limit on the possible

evolution of infrared galaxy luminosity function. Detailed modelling is in progress. But we are pessimistic about explaining the point-sources based on cold dust scenarios.

In conclusion, the point-like CBR anisotropy is a clear non-Gaussian signature. If the future studies confirm that the point sources candidates are truly CBR fluctuations, it will be an exciting new chapter. It will provide direct evidence that topological remnants left over from the early universe do exist.

8 Conclusion

In summary, the following points which are related to the test of the Gaussian nature of the primordial fluctuations are discussed in this paper:
(1) We listed the skewness and kurtosis in various physically motivated models, with and without noise. We also discussed the use of the multivariant skewness and kurtosis to quantify the deviation of a distribution from Gaussian.
(2) We discussed in detail the Euler-Poincare characteristic of random fields. We showed that the Euler-Poincare characteristic will not be a good discriminator between Gaussian and non-Gaussian random field when the noise is comparable to the signal.
(3) We stress the use of the three-point temperature correlation function to test Gaussianity. The predictions from various models are discussed and the COBE 53 Ghz data is analyzed. The analysis shows that the fluctuations are probably Gaussian on the COBE scale.
(4) We discussed the detailed statistical tests on intermediate angular scales. The bispectral analysis and Hotelling's T^2 statistics are emphasized. We also discussed briefly the sampling technique and minimum sample size to test Gaussianity statistically on half degree scales.
(5) We discussed testing Gaussianity on small angular scales (arcminute scales). The RING data from OVRO is analyzed and shown to be propably non-Gaussian.
(6) We discussed looking for point-like sources as a way to test Gaussianity and hunt for topological defects in small scale CBR experiments. The SZ effects and the effects of primeval dusts are discussed.

The current status of testing Gaussian nature of CBR anisotropies are summarized in Table 3.

Acknowledgments

I want to thank my advisor, David N. Schramm, for his constant encouragement and guidance over the years. I want to thank Stephan Meyer, Albert Stebbins, Neil Turok, George Smoot and Lyman Page for very helpful discussions. I also want to thank Roberta Bernstein and Brian Fields for reading and editing the paper. This work is support in part by NSF grant # 90-2269 and by NASA grant # NAGW 1321 at the University of Chicago and by DoE and by NASA through grant # NAGW 2381 at Fermilab. The COBE datasets were developed by the NASA Goddard Space Flight Center under the guidance of the COBE Science Working Group and were provided by the NSSDC.

Appendix

A Gaussian Nature of Perturbations from Inflation

In this appendix, we will discuss the Gaussianity of the primordial fluctuations produced in inflation. We pick one simple model, Linde's chaotic inflation model [51] to analyze. The approach is rather heuristic but brings into focus the Gaussianity problem. For more rigorous treatment, see [52].

The basics of the inflationary dynamics are the following: there exists an epoch where the universe is dominated by the vacuum energy of a scalar field ϕ. The Friedman equation which describes the evolution of the background metric is:

$$H^2 = \frac{8\pi G}{3}\rho, \quad \rho = 1/2\dot{\phi}^2 + V(\phi), \tag{85}$$

and the dynamical evolution of ϕ field is:

$$\ddot{\phi} + 3H\dot{\phi} + \frac{\partial V(\phi)}{\partial \phi} = 0, \tag{86}$$

where the inflaton potential for chaotic inflation is simply

$$V(\phi) = \lambda\phi^4. \tag{87}$$

The model is easy to analyze in the slow-roll regions where $\ddot{\phi} \ll H\dot{\phi}$, which is sastified for $\phi > m_{pl}/\sqrt{2\pi}$. By using the gauge-invariant parameter ζ introduced by [53], where

$$\zeta_k \approx \frac{H(\Delta\phi)}{\dot{\phi}}, \tag{88}$$

$\Delta\phi$ is the zero-point quantum fluctuation of the field ϕ along its classical trajectory. The probability density function for $\Delta\phi$ is a Gaussian with zero mean and variance given by $(\Delta\phi)^2 = (\frac{H}{2\pi})^2$. Let us denote $\frac{2\pi\Delta\phi}{H}$ by x, then x is a random variable with standard normal distribution.

Expressed in terms of x, ζ is given by:

$$\zeta_k = \frac{H^2}{\dot{\phi}} \cdot x \tag{89}$$

In the slow approximation, the quantum fluctuation of $\dot{\phi}$ is negligible. Thus, if the Hubble parameter is a constant during inflation (which is the case for original exponential inflation), one can conclude that the primordial density fluatuation is Gaussian. However, since H is related to ϕ locally, the fluatuation in ϕ will give rise to a fluctuation in H. Taking this into account,

$$\zeta_k = \frac{H_c^2}{\dot{\phi}}[x + \sqrt{\frac{\lambda}{12\pi}}\frac{\phi}{m_{pl}}x^2], \tag{90}$$

where H_c is the classical value and $m_{pl} = \frac{1}{\sqrt{G}}$ is the Planck mass. The usefulness of the ζ parameter lies in the fact that it is a constant throughout the inflationary, radiation and matter dominated epoch, and the Sachs-Wolfe contribution to the CBR temperature fluctuation is given by [52]:

$$\frac{\delta T}{T} \simeq \frac{\zeta}{5} \tag{91}$$

Thus, the large angular temperature anisotropy is given by:

$$\frac{\delta T}{T} \simeq \frac{H_c^2}{5\dot{\phi}}[x + \sqrt{\frac{\lambda}{12\pi}}\frac{\phi}{m_{pl}}x^2] \tag{92}$$

The statistics of CBR fluctuations are non-Gaussian because of the x^2 term. This expression for the deviation from Gaussianity is rather generic in inflationary models and will lead to the functional form of the three point correlation we will give in section 4. The difference is that various models will produce different skewness. In the one-field chaotic inflation model we treat now, the skewness is given by:

$$\mu_3 = 3\sqrt{\frac{\lambda}{12\pi}}\frac{\phi}{m_{pl}}. \tag{93}$$

During the slow roll [17],

$$\frac{H^2}{\dot{\phi}} = 4\sqrt{2/3}\lambda^{1/2}N_e^{3/2}, \tag{94}$$

where $N_e \sim 60$ is the number of $e-$folds the scale factor inflates during inflation. In order for the amplitude of the fluctuation to be of the same order

of magnitude as the COBE observation [8], the self-coupling constant λ of the inflaton field is given by $\lambda \sim 10^{-15}$. For such a weakly coupled field, the deviation from Gaussian is estimated to be: $\mu_3 \sim 10^{-7}$ with $\phi \sim \phi_i \sim 5m_{pl}$, which is negligibly small.

In conclusion, we have shown that the primordial fluctuation from slow roll inflation is very close to a Gaussian. The deviation from Gaussianity is of order 10^{-7} in the chaotic inflation model, and the result is general to other one-field inflation models. The root cause is the small coupling constant of the inflaton potential, which is required to give the right amplitude for primordial fluctuations. Thus, Gaussian-distributed CBR anisotropies are a nature result of lots of inflation models.

References

[1] A. Guth, *Phys. Rev. D* **23**, 347 (1981); A. Linde, *Phys. Lett. B* **108**, 389 (1982); A. Albrecht and P. J. Steinhardt, *Phys. Rev. Lett.* **48**, 1220 (1982).

[2] J. M. Bardeen, P. J. Steinhardt, and M. S. Turner, *Phys. Rev. D* **28**, 679 (1983); A. Guth and S-Y Pi, *Phys. Rev. Lett.* **49**, 1110 (1982); S. Hawking, *Phys. Lett. B* **115**, 295 (1982); A. A. Starobinskii, *Phys. Lett. B* **117**, 175 (1982).

[3] T.W.B. Kibble, *J. Phys.* **A9**, 1387 (1976).

[4] For a review, see A. Vilenkin, *Phys. Rep.* **121**, 263 (1985); N. Turok, *Phys. Rev. Lett.* **66** 2625 (1989).

[5] T.J. Allen, T.J., B. Grinstein, B. and M. B. Wise, *Phys. Lett. B* , **197**, 66 (1987); L. A. Kofman and A. D. Linde *Nucl. Phys.* **B282**, 555 (1985); Ortolan, A., Lucchin, F., and Matarrese, S. 1989, *Phys. Rev. D*, **40**, 290 (1989); D. S. Salopek, J. R. Bond, *Phys. Rev. D* **42**, 3936 (1990); D. S. Salopek, J. R. Bond, and G. Efstathiou, *Phys. Rev. D* **40**, 1753 (1989), H.M. Hodges, G.R. Blumenthal, L.A. Koffman and J.R. Primack, *Nucl. Phys.* **B335**, 197 (1990); D.S. Salopek, *Phys. Rev. D* **45**, 1139 (1992).

[6] D. H. Weinberg and S. Cole, *MNRAS*, in press (1993).

[7] X. Luo and D. N. Schramm, *Astrophys. J.* **408**, 33, (1993).

[8] G. Smoot *et al.*, *Astrophys. J.* **396**, L1 (1992); E. Wright *et al.*, *Astrophys. J.* **396**, L13 (1992); Bennett, C. *et al.*, *Astrophys. J.* **396**, L7 (1992).

[9] J.O. Gunderson *et al.* , *Astrophys. J.*, **413**, L1 (1993); P.R. Meinhold *et al.* CfPA Preprint (1993), to be published; M. Devlin, *et al.*, *Proc. Nat. Acad. Sci.*, **90**, 4774 (1993); M. Dragovan, Talk given at AAS meeting (1993); J. Schuster *et al. Astrophys. J.*, **412**, L47 (1993); E.S. Cheng et al. *Astrophys. J.* in press (1993); T. Gaier, *et al.*, *Astrophys. J.* **399**, L1 (1992); S.T. Meyers, A.C.S. Readhead, and C.R. Lawrence, CAL-TECH Preprint (RING experiment) (1992); E.J. Wollack *et al.*,

Preprint University Preprint (1993); J. Peterson, Talk given at ASPEN Physics Center (1993).

[10] P. Coles and J. D. Barrow, *MNRAS*, **228**, 407 (1987).

[11] F. R. Bouchet, D. Bennett, and A. J. Stebbins, 1988, *Nature*, **335**, 410 (1988).

[12] J. R. Bond and G. Efstathiou, *MNRAS*, 226, 655 (1987).

[13] K. Ganga, E. Cheng, S. Meyer, and L. Page, *Astrophys. J.* **410**, L57 (1993).

[14] P. Graham, N. Turok, P. M. Lubin and J. A. Schuster, PUP-TH-1408 (1993); D. Coulson, *et al.*, Princeton preprint PUP-TH-93/1393 (1993).

[15] X. Luo and D.N. Schramm, *Phys. Rev. Lett.* **71**, 1124 (1993).

[16] R. Moessner, L. Perivolarpoulos, and R. Brandenberger, Brown Univ. Preprint, BROWN-HET-911 (1993).

[17] E. Kolb and M. S. Turner, *The Early Universe* (Redwood City, Addison Wesley, 1990).

[18] W. Feller, *An Introduction to Probability Theory and Its Application*, **Vol.1&2** (New York, John Wiley and Sons, Inc., 1971).

[19] R.L. Scherrer and R. Schaefer, Ohio State University Preprint OSU-TA-7/92 (1992); L. Perivolaropoulos, Center for Astrophysics Preprint No. 3526, *Phys. Rev. D* , in press (1993).

[20] S.T. Meyers, A.C.S. Readhead, and C.R. Lawrence, CAL-TECH Preprint (RING experiment) (1992).

[21] J.O. Gunderson *et al.* , *Astrophys. J.*, **413**, L1 (1993); P.R. Meinhold *et al.* CfPA Preprint (1993), to be published; M. Devlin, *et al.*, *Proc. Nat. Acad. Sci.*, **90**, 4774 (1993); M. Dragovan, Talk given at AAS meeting (1993); J. Schuster *et al. Astrophys. J.*, **412**, L47 (1993); E.S. Cheng et al. *Astrophys. J.* in press (1993); T. Gaier, *et al.*, *Astrophys. J.* **399**, L1 (1992); E.J. Wollack *et al.*, Preprint University Preprint (1993); J. Peterson, Talk given at ASPEN Physics Center (1993).

[22] R. A. Sunyaev and Ya. B. Zeldovich, *Ann. Rev. Astro. Astrophys.*, **18**, 537 (1980).

[23] S. Cole and N. Kaiser, *MNRAS*, **233**, 637 (1988).

[24] N. Turok and D. N. Spergel, *Phys. Rev. Lett.* **66**, 3093 (1991); R.L. Davis, D.N. Spergel, N. Turok, and H. Collins, Princeton Univ. Preprint (1992).

[25] T.S. Rao and M.M. Gabr, *An Introduction to Bispectral Analysis and Bilinear Time Series Models*, Lecture Notes in Statistics, 24 (Springer, New York, 1980)

[26] R. J. Adler, *The Geometry of Random Fields*, (New York, John Wiley, 1981).

[27] J. M. Bardeen, J.M., J. R. Bond, J.R., N. Kaiser, N. and A. S. Szalay, A.S. 1986, *Astrophys. J.* **304**, 15 (1986).

[28] G. Smoot, Private communication (1993).

[29] P. Coles, *MNRAS*, **234**, 509 (1988).

[30] J.R. Gott III, C. Park, R. Juszkiezicz, W.E. Bies, D.P. Bennett, F.R. Bouchet, and A. Stebbins, *Astrophys. J.* **352**, 1 (1990).

[31] P. J. E. Peebles, *The Large-Scale Structure of the Universe* (Princeton, Princeton Univ. Press, 1980)

[32] N. Kaier, *Astrophys. J.* **284**, L9 (1984); Jensen, L.G., and Szalay, A.S., *Astrophys. J.* **305**, L5 (1986); D. Polizer and M. Wise, *Astrophys. J.* **285**, L1 (1984); P. Coles, *MNRAS*, **222**, 9p.

[33] E. H. Vanmarcke, *Random Fields: Analysis and Synthesis* (MIT Press, Cambridge, Massachusetts, 1983)

[34] X. Luo and D.N. Schramm, *Astrophys. J.* **408**, 33; Talk, T., Rangarajan, R., and M. Srednicki, *Astrophys. J.* **403**, L1 (1993); X. Luo and D.N. Schramm, *Phys. Rev. Lett.* **71**, 1124 (1993); Srednicki, M., 1993, CfPA-93-th-18, astro-ph/9306012.

[35] C. T. Hill, D. N. Schramm, and J. Fry, Comments Nucl. Part. Phys. **19**, 25 (1989); X. Luo and Schramm, Fermilab-Pub-93/020-A (1993); E. Kolb and Y. Wang, *Phys. Rev. D* **45**, 4421 (1992).

[36] A. M. Polyakov, *JEPT lett.*, **12**, 538 (1970).

[37] M. SubbaRao, A. Szalay, R. Schaefer, S. Gulkis, and P. von Gronefeld, John Hopkins Preprint 147 (1993).

[38] A. Kogut, *et al.*, COBE Preprint 93-07 (1993).

[39] L. F. Abbot and M. Wise,*Astrophys. J.* **282**, L47 (1984); R. Scaramella and N. Vittirio, *Astrophys. J.* **353**, 372 (1990); R. Scaramella and N. Vittorio,*Astrophys. J.* **375**, 439 (1991); M. White, L. Krauss and J. Silk, *Astrophys. J.* submitted, astro-ph/9303009 (1993).

[40] E.S. Cheng *et al.*, *Astrophys. J.* in press (1993).

[41] J. Schuster *et al. Astrophys. J.*, **412**, L47 (1993)

[42] D. R. Brillinger, *Times Series, Data Analysis and Theory* (Holt, Rinehart and Winston, New York, 1975).

[43] D. Scott, M. Srednicki and M. White, *Astrophys. J.* in press (1993).

[44] E.J. Wollack *et al.*, Preprint University Preprint (1993).

[45] K. Gorski, *Astrophys. J.* **410**, L65 (1993).

[46] G. Goetz and D. Nötzold, *Phys. Rev . Lett.* **65**, 2229 (1990); M. S. Turner, R. Watkins, and L. Widrow, *Astrophys. J.* **367**, L47 (1991).

[47] D. Bennett and Rhie, S., *Phys. Rev. Lett.* **65**, 1709 (1991).

[48] J. R. Bond, B. J. Carr, and C. J. Hogan, *Astrophys. J.* **306**, 428 (1986).

[49] C.A. Beichman and G. Helou, *Astrophys. J.* **370**, L1 (1991).

[50] J.C. Mather, *et al.*, COBE Preprint 93-01 (1993); E. Wright, *et al.*, COBE Preprint No. 93-03 (1993).

[51] A.D. Linde, 1983, *Phys. Lett. B* , **129**, 177 (1983).

[52] D.S. Salopek, J.R. Bond, and G. Efstathiou, *Phys. Rev. D* **40**, 1753 (1989).

[53] J.M. Bardeen, P.J. Steinhardt, and M.S. Turner, *Phys. Rev. D* **28**, 679 (1983).

Table Captions

Table 1: The skewness and kurtosis of the temperature anisotropies in various non-Gaussian models.

Table 2: Testing the properites of signal and noise in COBE 53 GHz map. W_n is the statistic for testing mutual independence of noise. Under the null hypothesis that the noise is uncorrelated, W_n will distribute as a standard normal. W_c is for testing correlation between signal and noise, and W_s is for testing the correlation between signals. Under the null hypothesis (signal and noise are not correlated; signals are not correlated), both W_c and W_s are distributed as standard normals.

Table 3: A summary of current status on testing Gaussian nature of CBR temperature anisotropies on different angular scales.

Table 1

Non-Gaussian Sources	No Noise		Signal to Noise Ratio 1:1	
	Skewness	Kurtosis	Skewness	Kurtosis
Soft Domain Wall[1]	1.4	3.75	0.5	0.94
Cosmic string[2]	0	1.5	0	0.38
Global monopole[3]	0.82	1.25	0.29	0.31
Global Texture[3]	0.71	0.94	0.25	0.25
$O(N)$ σ-model[3]	$\sqrt{2/N}$	$15/4N$	$\sqrt{1/4N}$	$15/16N$
SZ from Rich Cluster[4]	-0.66	2.72	-.28	0.22

[1] Extrapolated from $O(N)$ model
[2] On Scales of several arcminutes
[3] COBE sensitive scale, no beam-smoothing
[4] On Scales of several arcseconds to arcminutes

Table 2

	estimate	Confidence Level
W_n	2.54	1.58×10^{-2}
W_c	1.21	0.19
W_s	8.73	1.1×10^{-17}

Table 3

Angular scale θ_s	Small ($\sim$ arcminutes)	Intermediate ($\sim 1°$)	Large ($\gg 2°$)
Current Experiments	OVRO	South Pole, MAX, MSAM, SK93, PATHON, White Dish,...	COBE MIT balloon
Theoretical expectations	Non-Gaussian	Inflation: Gaussian; Defects: non-Gaussian.	Gaussian
Analysis from experiments	Non-Gaussian	Sky coverage is still too small	Gaussian
Comments	Source contaminations	Eventually Decisive	Central limit theorem; . Cosmic variance

Figure Captions

Fig. 1: The probability distribution functions of the modified χ^2 distribution with n degrees of freedom. The dotted line is for n=4, the short dash line is for n=8, the lone dash line is for $n = 16$ and the solid line is the standard normal distribution. The values for n are chosen because the corresponding distributions describe the domain wall, global string and texture, respectively.

Fig. 2: The simulated unsmoothed Gaussian noise δ in a $10^\circ \times 10^\circ$ patch. The solid line is for the contour $\delta = 0$, the dotted line is for the contour $\delta = \sigma$ and the short-dashed line is for $\delta = 2\sigma$, where σ is the standard deviation of the noise.

Fig. 3: The statistic of EP characteristic for a Gaussian random field. The soild line is the mean EP characteristic and the dotted line is the 1σ uncertainty estimated from Eq. (35). The unit of the vertical axis is arbitary.

Fig. 4a: The contour plot of the sky signals δ if they are dominated by a quadrupole. The solid line is for the contour $\delta = 0$, the dotted line is for the contour $\delta = \pm\sigma$ and the short-dashed line is for $\delta = \pm 2\sigma$, where σ is the standard deviation of the observed sky signals.

Fig. 4b: The contour plot of the sky signal δ when the signal to noise ratio is 1:1, where the signal is a quadrupole. The solid line is for the contour $\delta = 0$, the dotted line is for the contour $\delta = \pm\sigma$ and the short-dashed line is for $\delta = \pm 2\sigma$, where σ is the standard deviation of the observed sky signals.

Fig. 5: The genus curve for χ^2 distributions with n degrees of freedom. The solid line is for the random Gaussian field, the dotted line is for $n = 12$ and the dashed line is for $n = 21$, which describes the noisy case.

Fig. 6: The theoretical prediction of reduced three-point function in three different models: The dotted line is for inflation, the short dash line is for $O(N)$ σ model and the long dash line is for LTPT. The reduced two point function, which is the solid line, is modeled as $\exp(-\theta^2/\theta_c^2)$, where $\theta_c = 13.5^\circ$.

Fig. 7a: The reduced three point-functions estimated from COBE DMR 53 GHz (A+B)/2 map and (A-B)/2 map. The solid line is for the (A+B)/2 map and the dotted line is for the (A-B)/2 map.

Fig. 7b: The estimate and error of the three point function for COBE 53 GHz (A+B)/2 map. The result is consistent with prediction from a Gaussian field (which is zero).

Fig. 8a: The reduced three-point function estimated from RING data. We place 96 RING data points on a one dimensional lattice and the horizontal axis is the number of lattice spacing between the points used for estimating

the reduced three point function.
Fig. 8b: The plot of the real part of the estimated bispectrum $f(\omega_1, \omega_2)$ estimated from the RING data. In this plot, we choose $\omega_1 = \omega_2 = \omega$. The frequencies ω is plotted in unit of $\pi/20$.
Fig. 8c: The imaginary part of the estimated bispectrum $f(\omega_1, \omega_2)$ from the RING data. In this plot, we choose $\omega_1 = \omega_2 = \omega$. The frequency ω is plotted in units of $\pi/20$.
Fig. 9: The statistical distribution of $F = \frac{2(n-P)}{2P} T^2$. We choose $P = 2$ and $n = 9$ for the RING data.
Fig. 10: The frequency dependence of the antenna temperature for CBR and for SZ effect. The soild line is for CBR and the dotted line is for SZ. The antenna temperature is normalized so that it is unity at low frequencies.
Fig. 11: The flux density of the 4K cold dust. The emissivity of the dust is chosen to be $\approx \nu^{1.5}$. The unit of the vertical axis is arbitary.

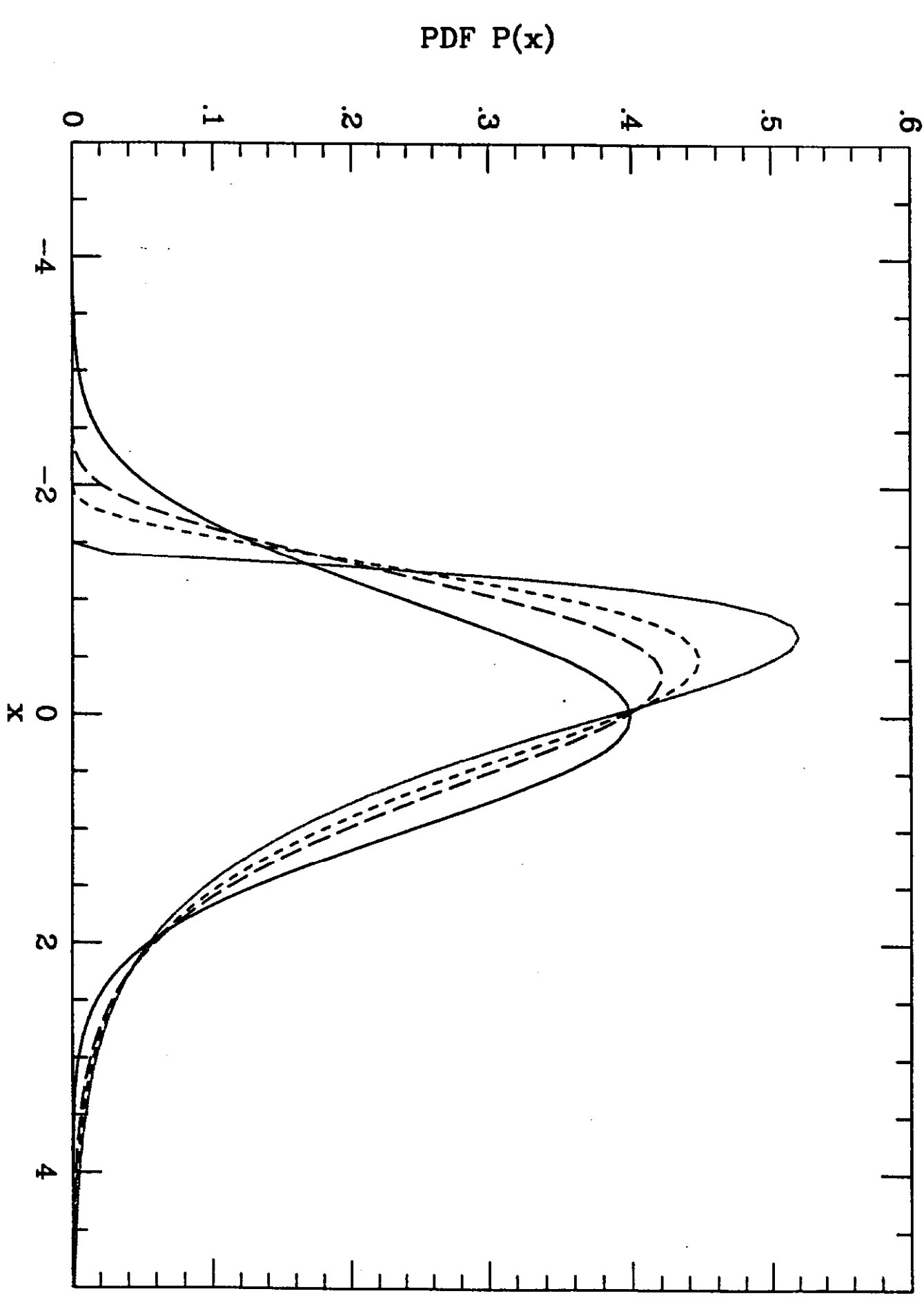

Figure 1

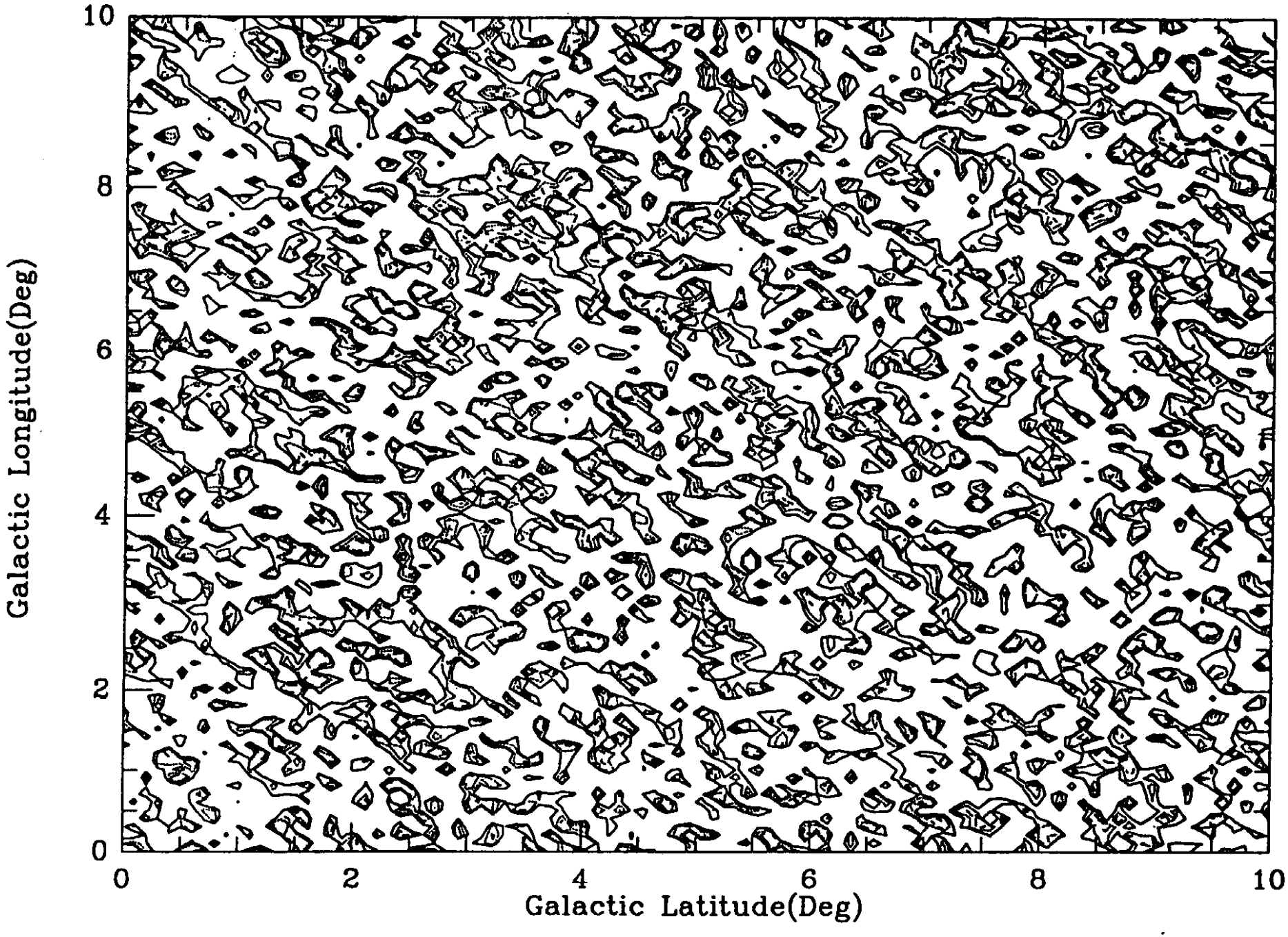
10
8
6
4
2
0
Galactic Longitude(Deg)
0
2
4
6
8
10
Galactic Latitude(Deg)

Figure 2

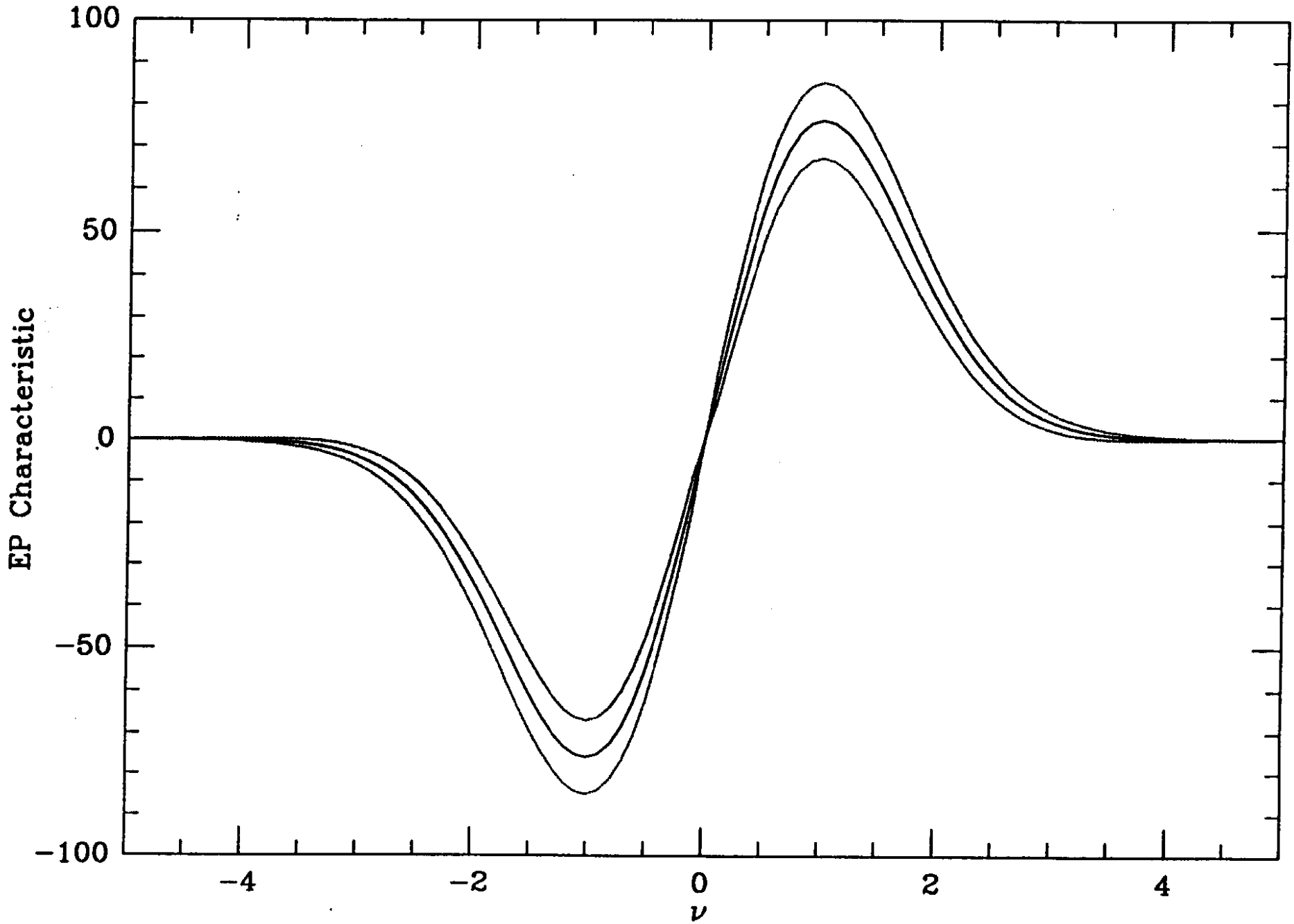

Figure 3

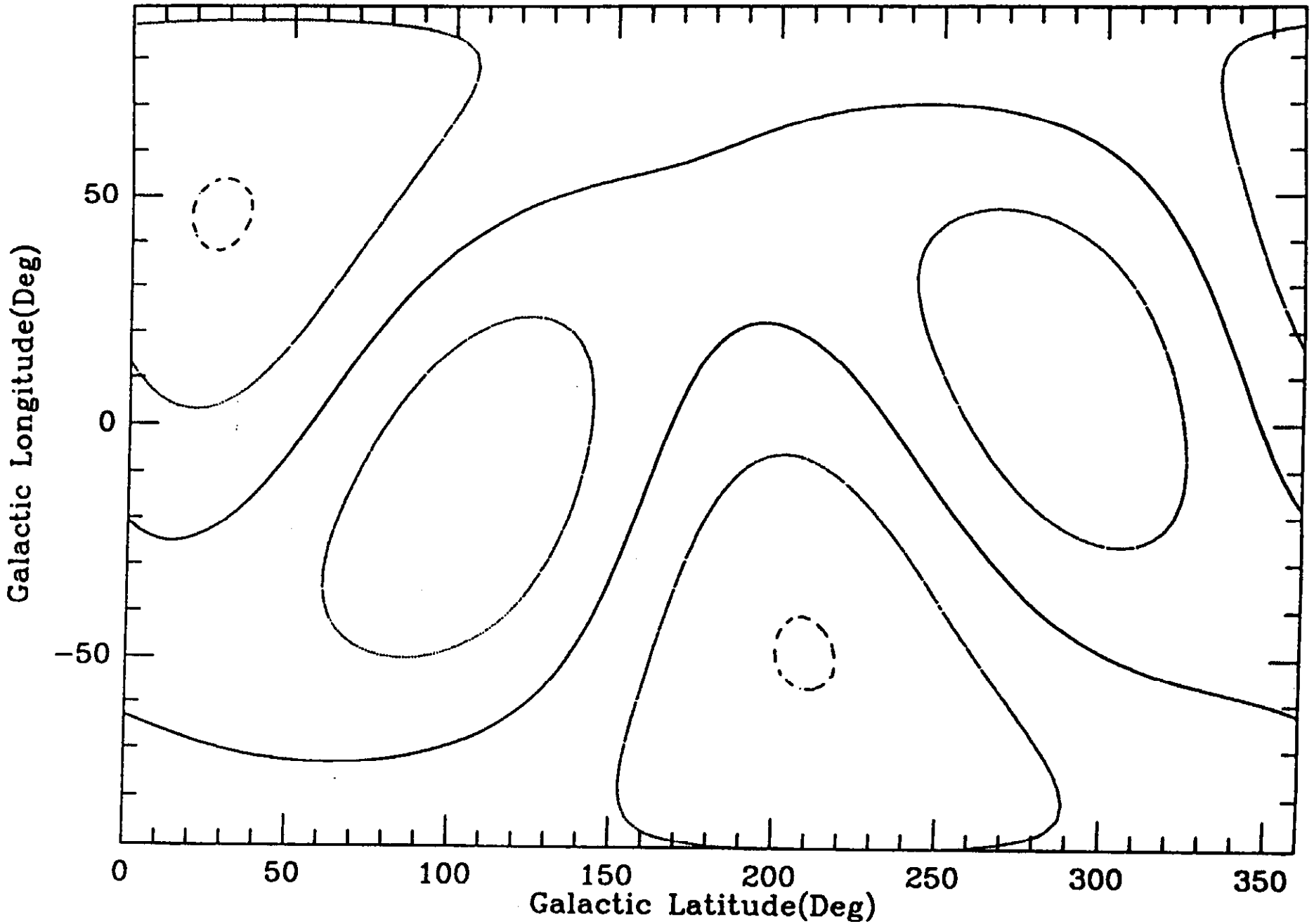
Galactic Longitude(Deg)
50
0
−50
0
50
100
150
200
250
300
350
Galactic Latitude(Deg)

Figure 4a

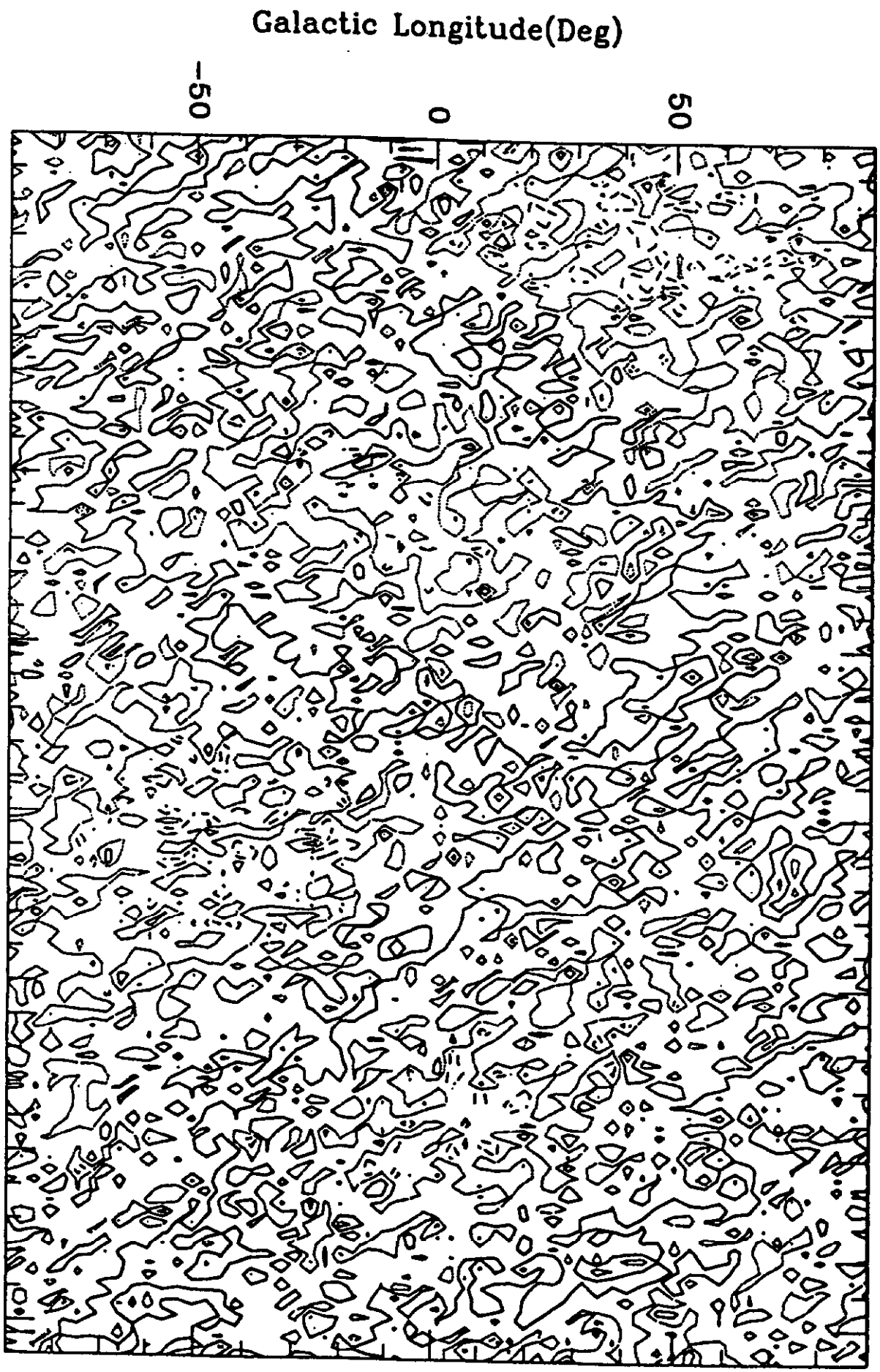
Galactic Longitude(Deg)
-50
0
50
0
50
100
150
200
250
300
350
Galactic Latitude(Deg)

Figure 4b

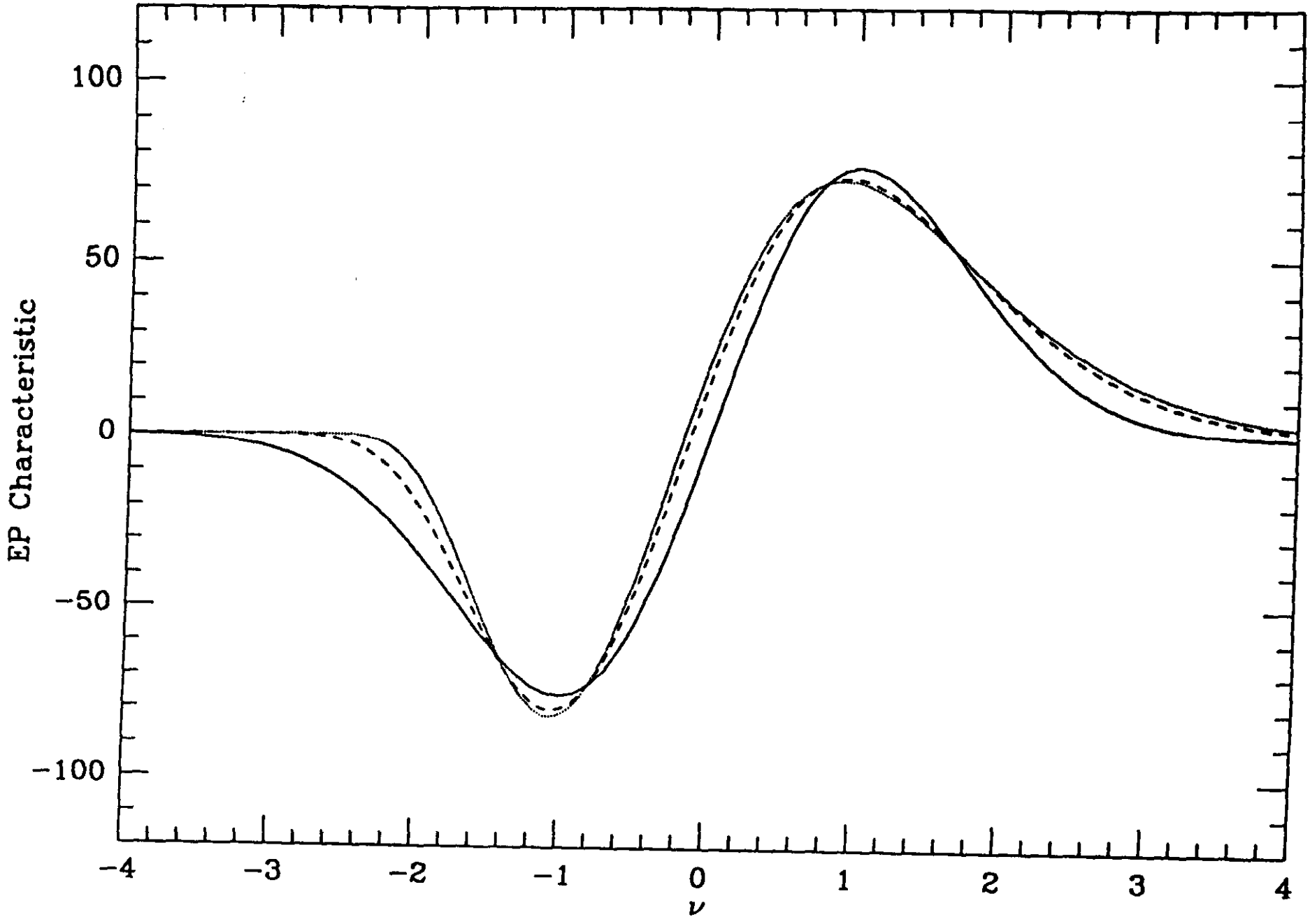

Figure 5

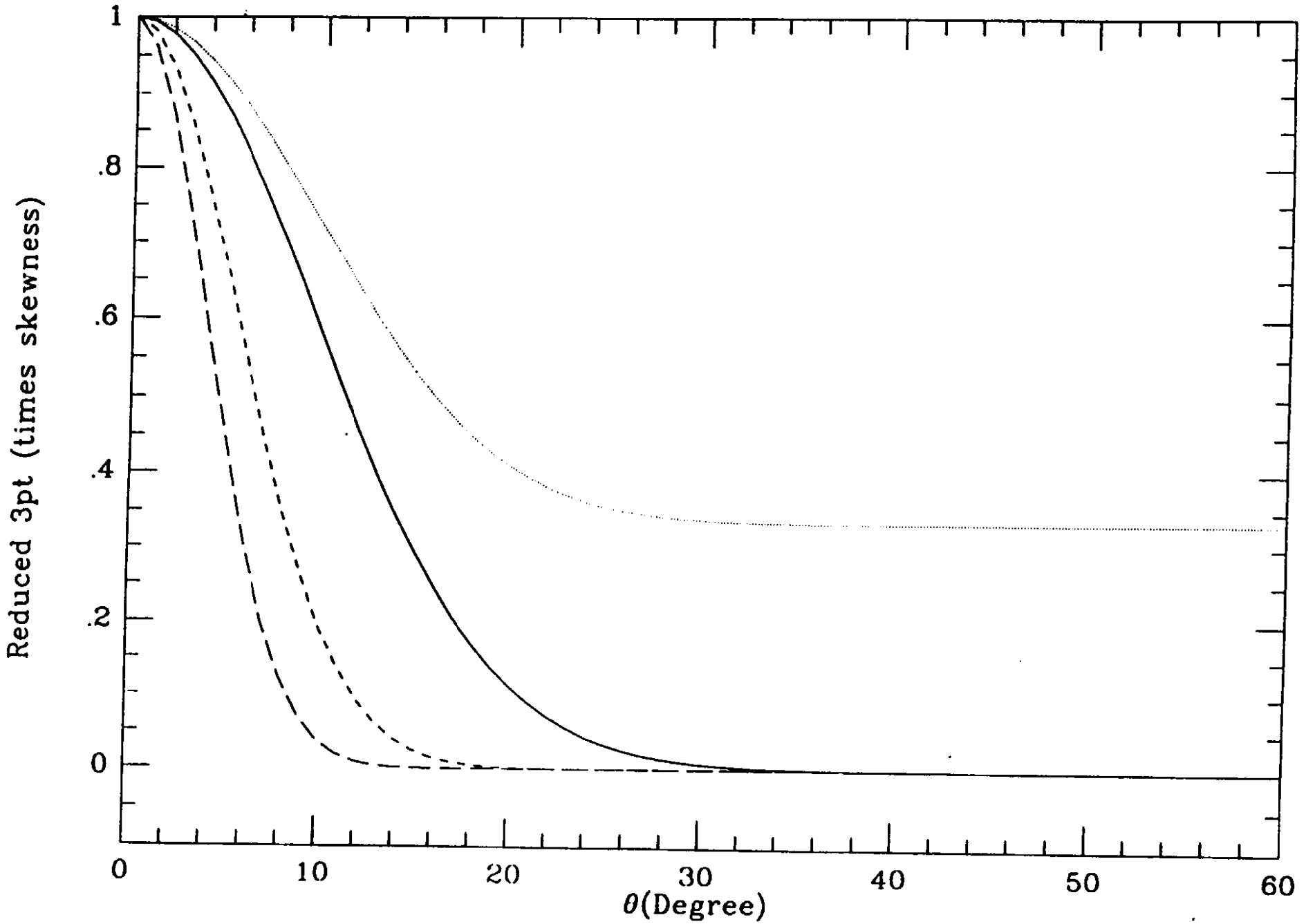

Figure 6

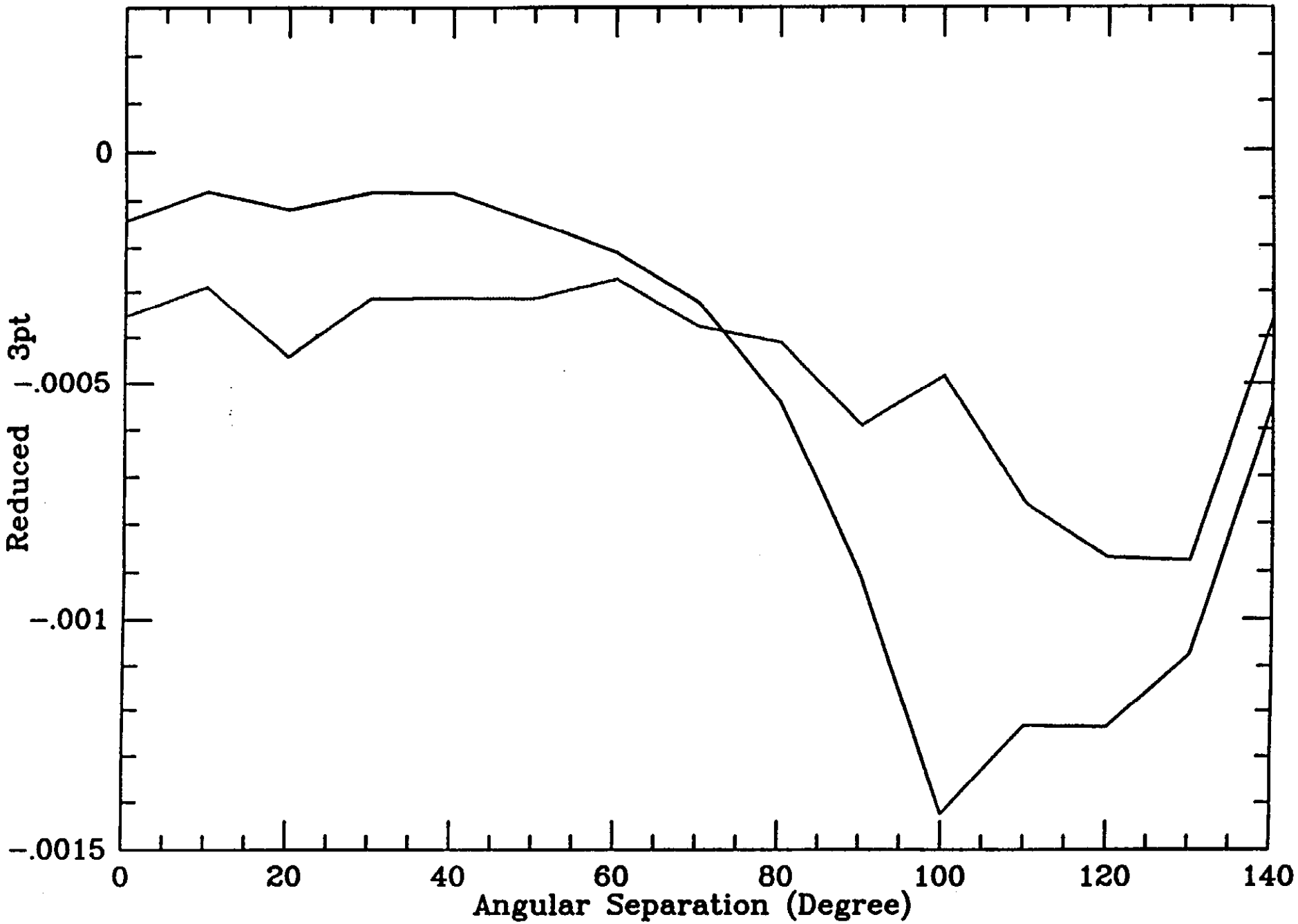
0
-.0005
-.001
-.0015
Reduced 3pt
0
20
40
60
80
100
120
140
Angular Separation (Degree)

Figure 7a

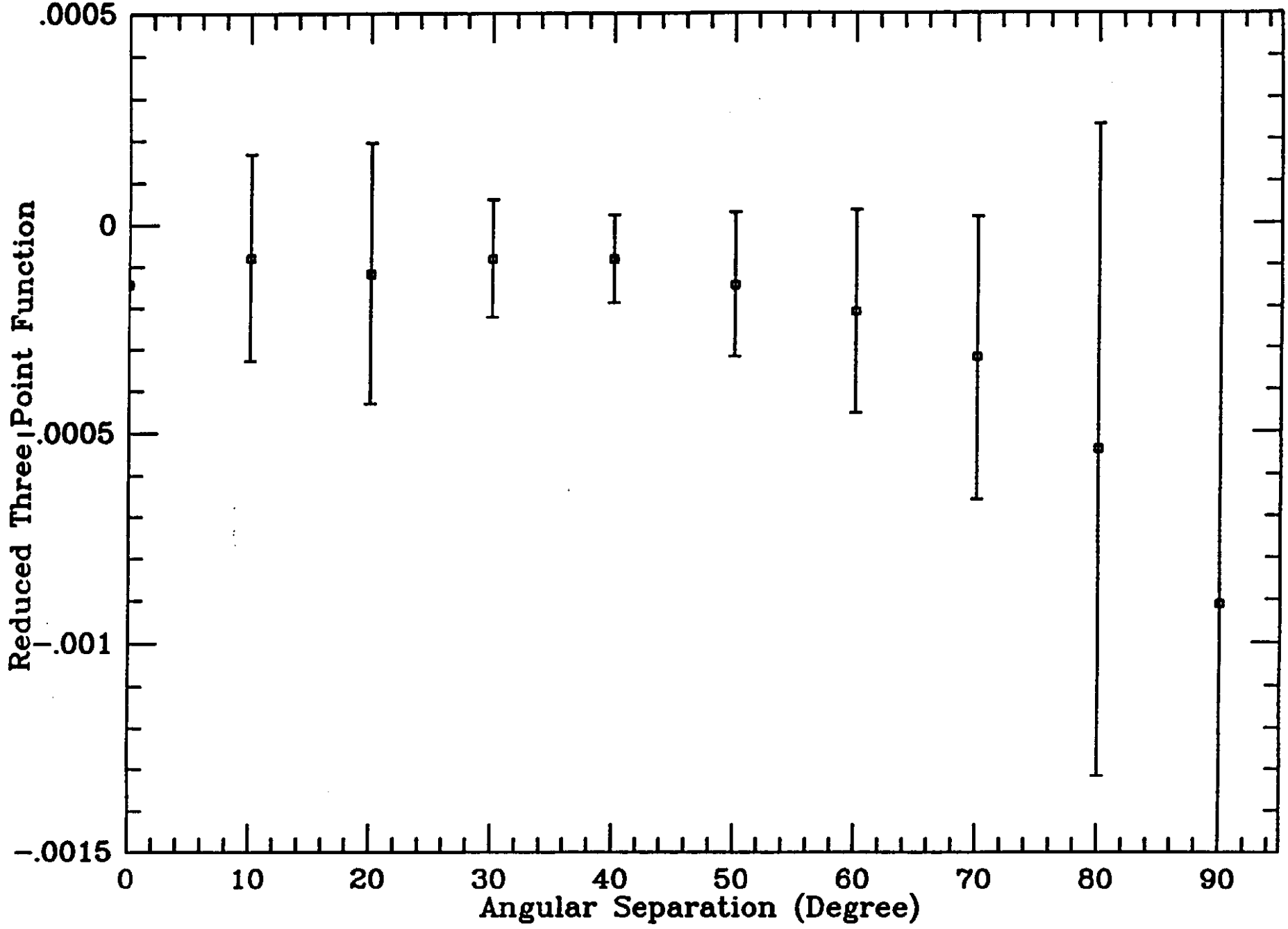
.0005
0
-.0005
-.001
-.0015
Reduced Three Point Function
0
10
20
30
40
50
60
70
80
90
Angular Separation (Degree)

Figure 7b

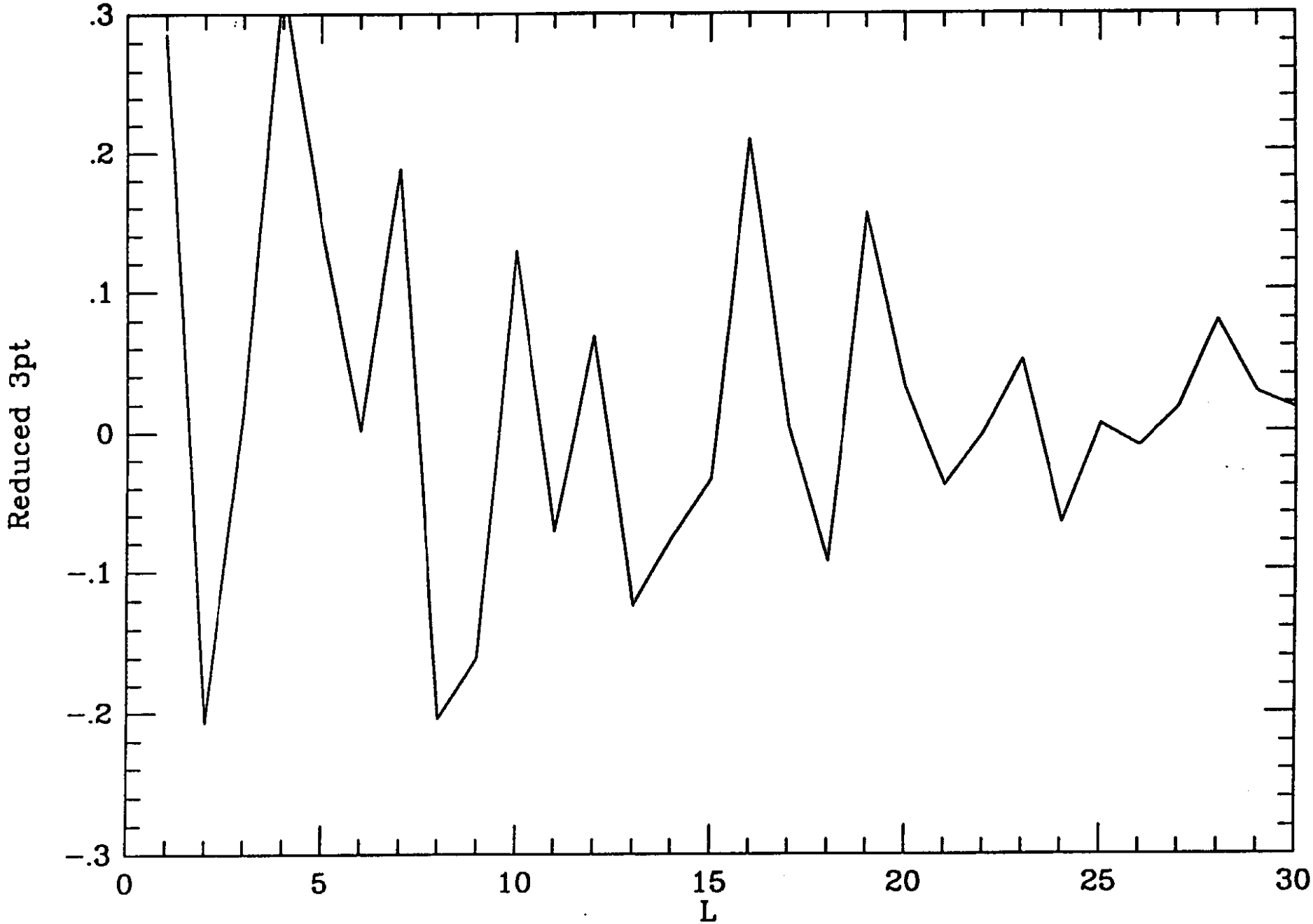

Figure 8a

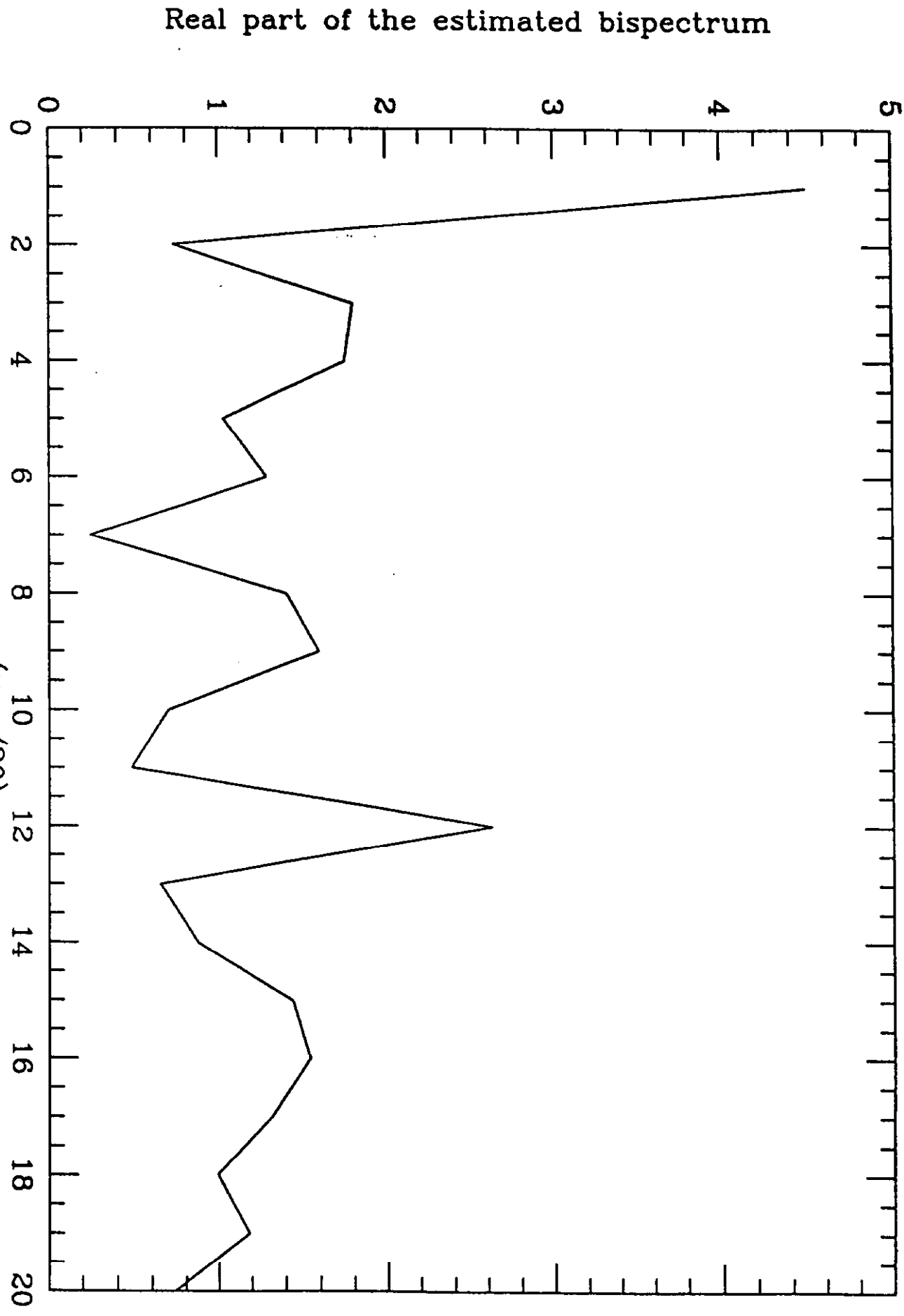
Real part of the estimated bispectrum
0
1
2
3
4
5
0
2
4
6
8
10
12
14
16
18
20
ω (× π/20)

Figure 8b

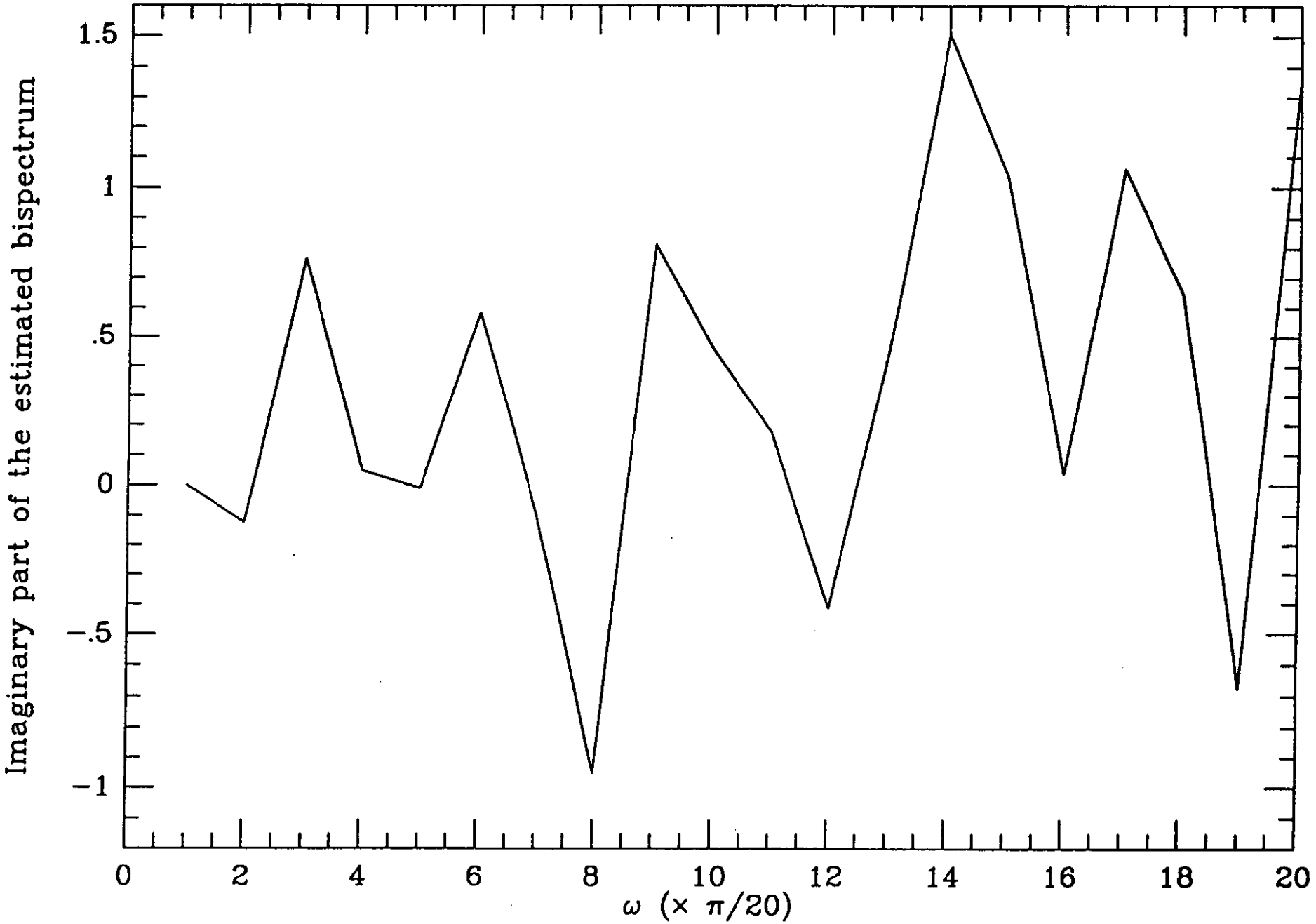
Imaginary part of the estimated bispectrum
1.5
1
.5
0
-.5
-1
0
2
4
6
8
10
12
14
16
18
20
ω (× π/20)

Figure 8c

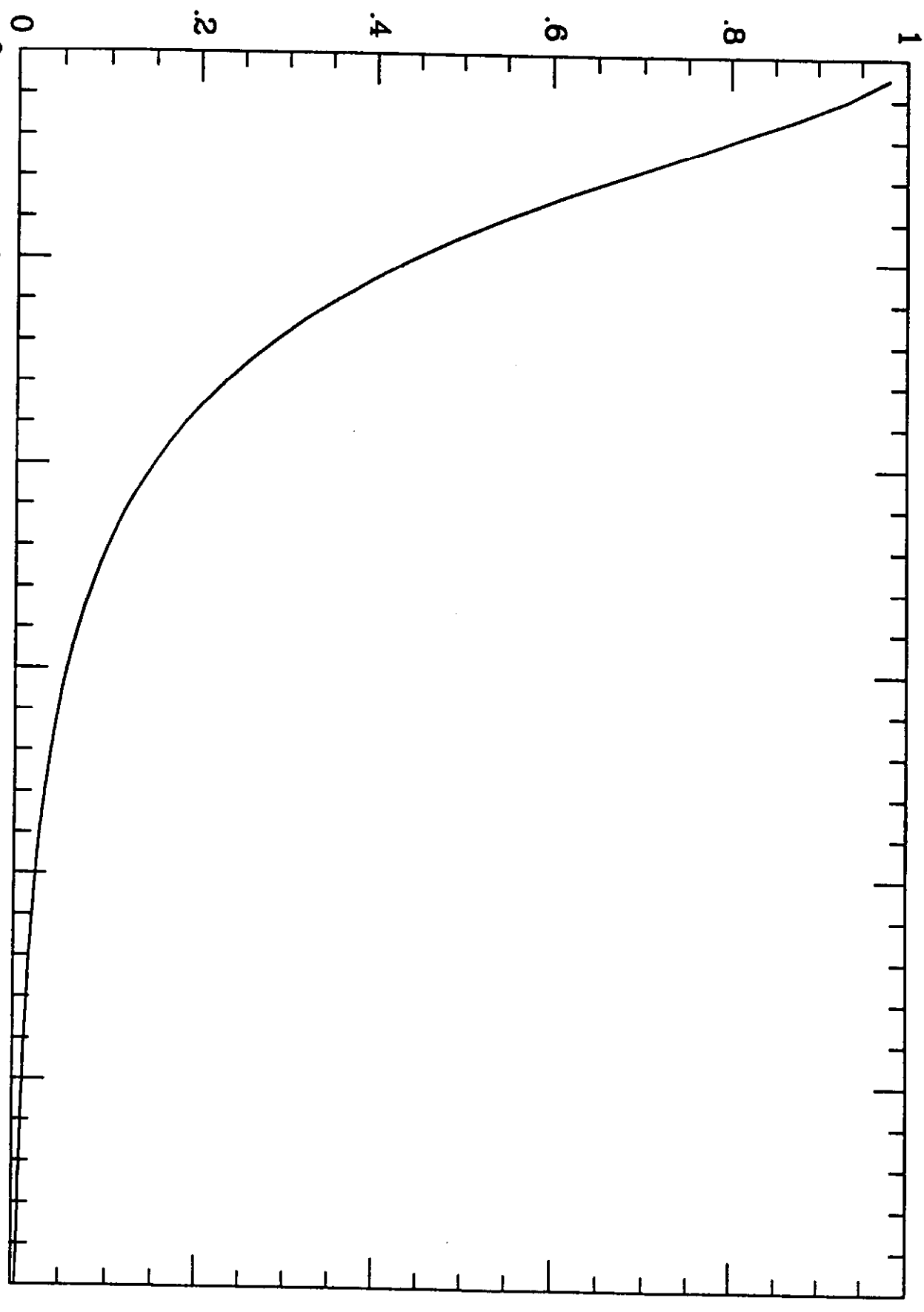

Figure 9

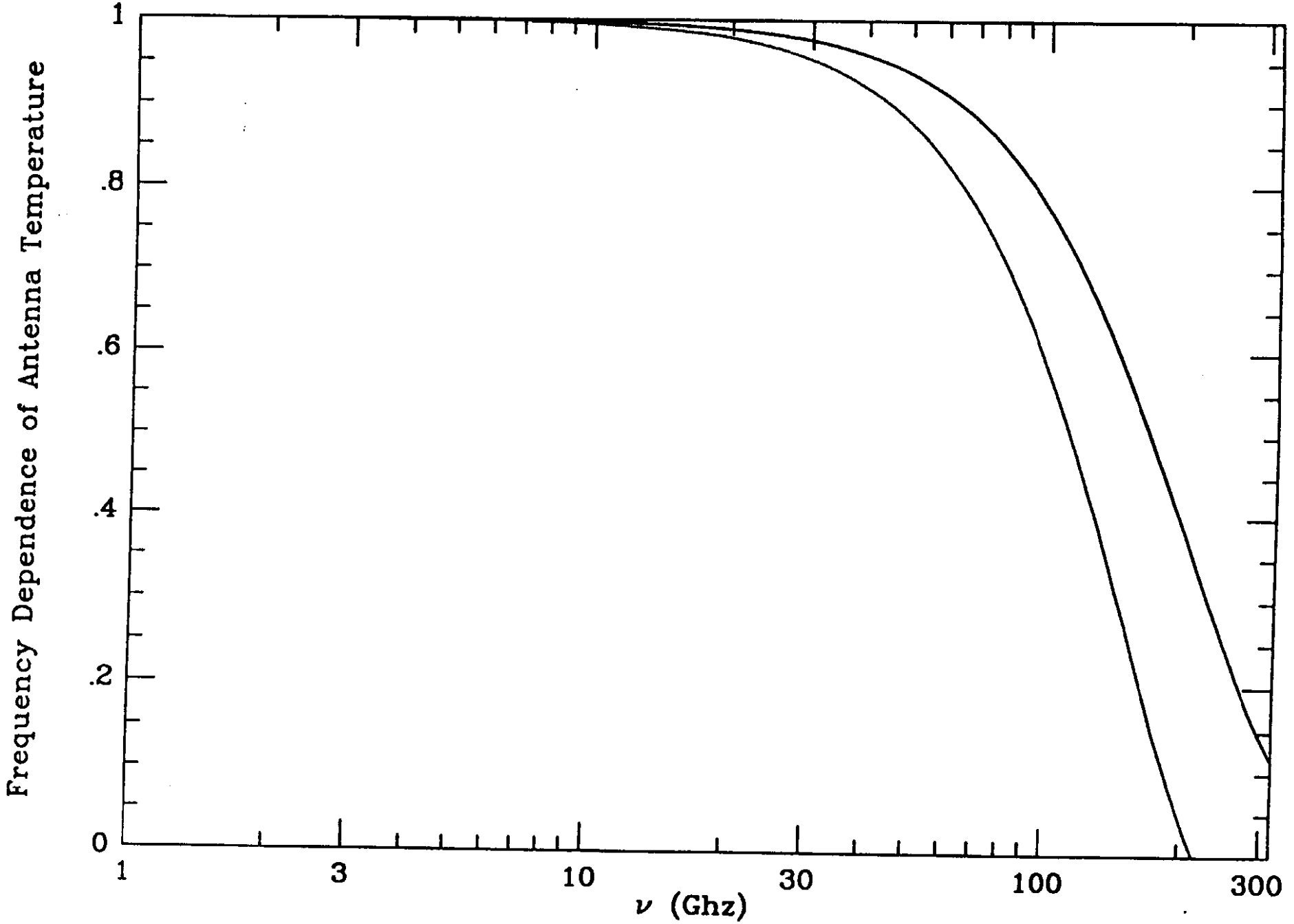
Frequency Dependence of Antenna Temperature
1
.8
.6
.4
.2
0
1
3
10
30
100
300
ν (Ghz)

Figure 10

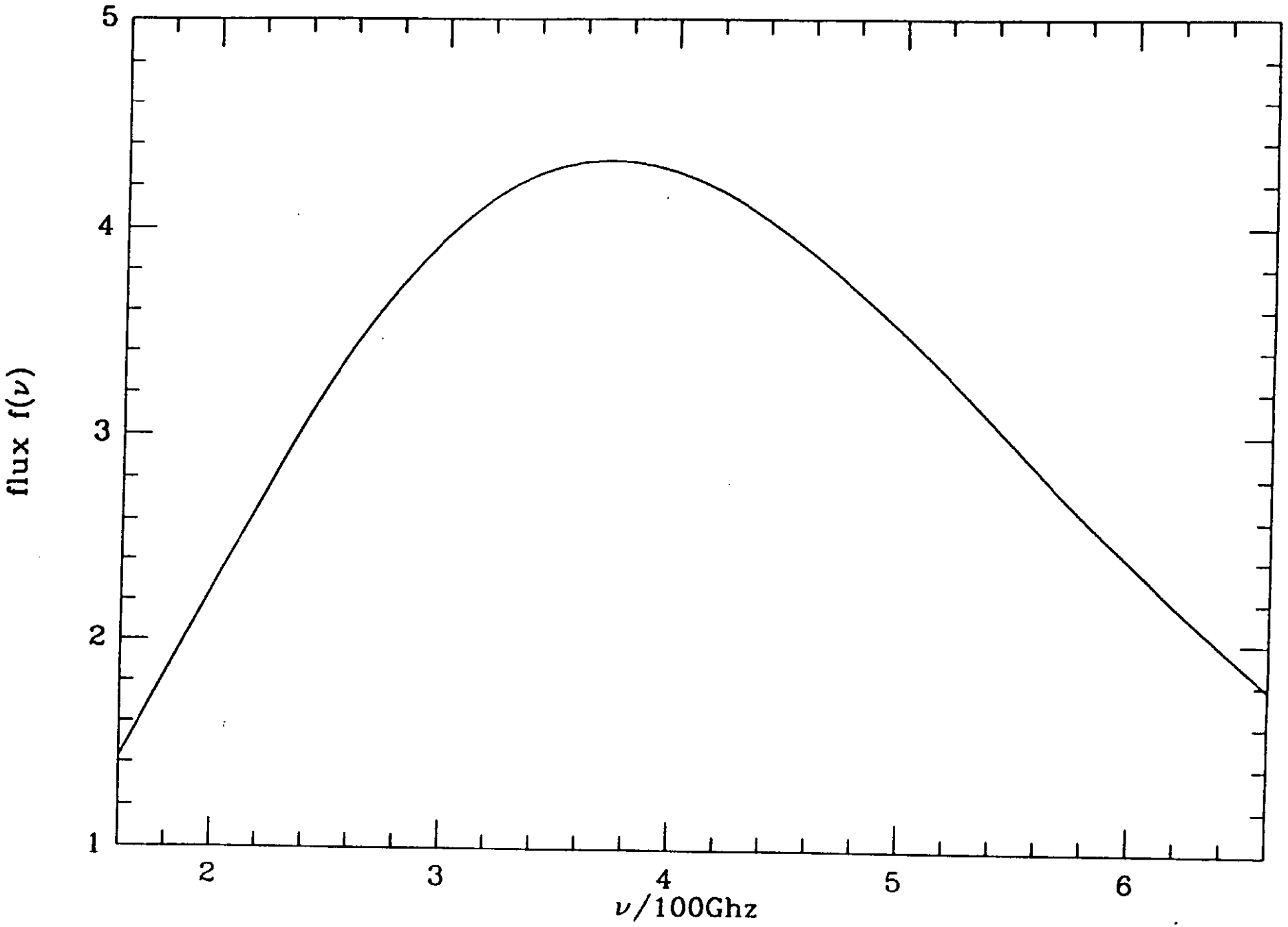

Figure 11